POLITECNICO DI TORINO

Collegio di Ingegneria Chimica e dei Materiali

Corso di Laurea Magistrale

in Ingegneria Chimica e dei Processi Sostenibili

Tesi di Laurea Magistrale

Explosibility and flammability of olive pomace dust

Supervisori

prof. Luca Marmo

prof. Paul Amyotte

firma dei relatori

Candidato

Matteo Pietraccini

firma del candidato

Marzo 2019

Index

Prefazione

2.2 Characterization analyzes

2.3 Explosibility and flammability analyzes

3. Results

3.1 Characterization analyzes results

3.2 Explosibility and flammability analyzes results

4. Discussion

4.4 Influence of the ignition source on samples explosibility and flammability

7. Annex

Prefazione

1. Introduzione

È un dato di fatto e conoscenza comune che il mar Mediterraneo è una regione ricca e adatta alla crescita di differenti specie vegetali, così come alla produzione di moltissimi prodotti da essi derivanti. Tra le attività tipiche di questa regione vi è la coltivazione degli ulivi, dai quali è possibile ottenere numerose qualità di oli d'oliva e olive. La zona mediterranea è responsabile della produzione di circa il 98% della produzione mondiale di olio di oliva, che conta 900 milioni di ulivi che occupano 10 milioni di ettari [1]. Inoltre, da ogni 100 kg di olive è possibile produrre circa 60 kg di olio di oliva [1], il che lo rende un'importante risorsa economica, culturale e politica, soprattutto per i paesi che si affacciano sul Mar Mediterraneo. Tuttavia, la manipolazione di 100 kg di olive per la produzione di olio di oliva è intrinsecamente legata alla produzione di 40 kg di rifiuti solidi [1], che può rappresentare un costo non irrisorio per un'azienda. È in quest'area che entra in gioco un sistema di valorizzazione, che può trasformare questi rifiuti di biomassa in una preziosa risorsa.

I sottoprodotti relativi alla produzione di olio di oliva sono principalmente tre: rami e foglie caduti nelle reti di raccolta delle olive e separati prima della molitura; l’effluente acquoso proveniente dal lavaggio delle olive e dall'acqua usata nel processo di estrazione; il residuo solido ottenuto dopo la decantazione/centrifugazione, formato in maniera predominante da pelle, nocciolo e polpa delle olive. Quest'ultimo sottoprodotto è chiamato sansa di oliva, al giorno d'oggi usato come mangime per animali, ammendante per terreni, fonte di olio di oliva nei processi di estrazione con solvente (per ottenere olio di sansa di oliva) e combustibile solido per i bruciatori a polvere, usati per ottenere energia termica [2]. Tuttavia, esistono molti altri progetti che prevedono l'uso di sansa di oliva in differenti settori: realizzazione di materiali da costruzione [3], produzione di biodiesel [4], rimozione del contenuto fenolico nelle acque di scarico dei frantoi [5], adsorbimento di coloranti [6] e molti altri. In ogni caso, il suo uso come combustibile in impianti di gassificazione, pirolisi e combustione sembra il più promettente al giorno d’oggi e in futuro, soprattutto a causa dell’aumento della domanda mondiale di nuove fonti energetiche e della ricercar in questo campo.

Ciò nonostante, la crescente produzione di bioenergia ha portato come diretta conseguenza l’aumento del pericolo ad essa legato. Infatti, come può essere notato nella Fig. 1.2, il numero di incidenti (normalizzati secondo l’energia netta prodotta) dal biennio 1996-98 a quello 2011-2013 è aumentato circa sette volte [8], considerando solamente l’energia prodotta da biomassa, e più di quattro volte considerando anche l’energia prodotta da biofuel e biogas (indicata come *bioenergy* in Fig. 1.2). Oltretutto, è proprio l’area della biomassa l’origine della maggior parte degli incidenti nel settore della bioenergia. Per questa ragione, il potenziale e crescente uso della sansa di oliva nell’industria deve includere lo studio del pericolo legato alla sua manipolazione, in realtà come silos (potenziale formazione di polverino fine), reattori di pirolisi o gassificazione (potenziale formazione di nubi di polvere in ambiente ad alta temperatura), depositi indesiderati in impianti di triturazione o macinatura (potenziale contatto con superfici calde e dispersione in nube). Queste situazioni sono solo alcune di quelle potenzialmente presenti in un’industria e possono portare a incendi e/o esplosioni, con severe conseguenze su impianti, lavoratori e persone presenti nelle vicinanze. Inoltre, la letteratura scarseggia in informazioni relative alla manipolazione sicura della sansa di oliva, perciò uno degli obiettivi di questo studio è anche la raccolta di informazioni a riguardo.

In questo lavoro, il campione di sansa di oliva analizzato (Fig. 2.1a) proviene dalla Spagna e si trova sottoforma di pellet. Visto che in questa forma la sansa di oliva non pone più problemi di un cumulo di materiale legnoso, l'analisi dei rischi è stata concentrata sulla polvere di sansa di oliva, la forma più pericolosa trovabile in una realtà industriale. Questo studio è stato sviluppato analizzando 4 campioni provenienti dalla stessa sansa ma con dimensioni particellari diverse, scelte per avere una buona rappresentazione di particelle grossolane, intermedie e fini. Siccome quando la dimensione particellare è bassa le polveri presentano fenomeni come formazione di aggregati e intense forze di coesione interparticellari, come rappresentanti dei fini sono state scelti due valori. Quelli finali sono: 400, 200, 80 e 45 µm.

Per conoscere la natura dei 4 campioni e del pellet, è stata fatta una caratterizzazione chimico-fisica determinando:

- L'umidità
- La distribuzione granulometrica
- La forma e l'aspetto delle particelle, attraverso un'investigazione SEM (Scanning Electronic Microscope)
- Il comportamento termico, attraverso un'analisi termo-gravimetrica
- Il contenuto lignocellulosico, attraverso una solid-state ^{1}H-NMR (^{1}H-Nuclear Magnetic Resonance)
- Il potere calorifico
- La densità in cumulo

Per quanto riguarda l'analisi dei rischi legati all'esplodibilità e all'infiammabilità dei campioni, i parametri determinati sono stati:

- Temperature minima di auto-ignizione (MAIT)
- Energia minima di ignizione (MIE)
- Concentrazione minima esplodibile (MEC)
- Parametri di esplosione (P_{max}, $(dP/dt)_{max}$ and K_{St})

2. Materiali e analisi

Il campione pellettizzato è stato macinato e polverizzato, poi vagliato per ottenere i quattro campioni. In base alla loro disponibilità, i setacci usati presentavano le seguenti dimensioni delle maglie: 425, 212, 75 and 45 µm. Le frazioni ottenute sono state le seguenti: quella compresa tra 425 e 212 µm (campione A), tra 212 e 75 µm (campione B), tra 75 e 45 µm (campione C) e quella minore di 45 µm (campione D). In seguito, sono state sottoposte ad essiccamento in un forno ventilato a 110°C per 24 h per raggiungere un'umidità minore del 5%wt (come enunciato nella procedura standard ASTM E1226-12a). In Fig. 2.1 sono riportate le immagini dei 4 campioni dopo la preparazione e l'immagine del campione pellettizzato di partenza.

La determinazione dell'umidità è stata eseguita con un Sartorius Moisture Meter MA e le misurazioni sono state ripetute tre volte per ottenere una buona accuratezza dei risultati.

La distribuzione granulometrica è una caratteristica fondamentale per la caratterizzazione di una polvere. la curva ottenibile può essere cumulativa o gaussiana ed è riportata in funzione del diametro particellare. L'analisi è stata effettuata con un Microtrac S3500, accoppiato a un Microtrac Turbotrac per la dispersione della polvere.

L'investigazione SEM permette di descrivere ed osservare la forma delle particelle e l'eventuale presenza di strutture peculiari o agglomerati. Prima di essere sottoposte ad analisi con il microscopio elettronico, le particelle vanno ricoperte da uno strato conduttore (in questo caso, 20 nm di oro-palladio): questa fase è stata portata a termine con un Low Vacuum Coater Leica EM ACE200 (intensità di corrente di 20 mA, tempo di esposizione di 260 s, pressione di 0,04-0,08 bar). L'investigazione SEM è stata effettuata in un Hitachi S-4700 Field Emission Scanning Electron Microscope, usando un potenziale di 10 kV.

L'analisi termo-gravimetrica permette di ottenere informazioni sul comportamento termico del campione (almeno quando sottoposto ad un riscaldamento lento e regolare), in particolare come varia la sua massa all'aumentare della temperatura. In questo modo, fenomeni come disidratazione, reazioni di pirolisi, ossidazione e combustione sono resi ben evidenti. Con i risultati della TGA, è possibile ottenere una proximate analysis del campione, cioè la sua umidità, materia volatile, carbone fisso e ceneri (le formule usate sono riportate nella Tab. 2.1). Oltretutto, conoscere materia volatile e carbone fisso significa avere un'idea della reattività del campione, associate al rapporto tra i due [19]. Questa analisi è stata effettuata con un Q600 SDT (Simultaneous Differential Technique), con una velocità di riscaldamento di 10°C/min, una temperatura finale di 1000°C, sia in aria che in argon.

Per conoscere il contenuto lignocellulosico dei campioni, è stata scelta una solid-state NMR, cioè una risonanza magnetica nucleare con campione allo stato solido. È infatti possibile ottenere informazioni circa la concentrazione di specifiche molecole o classi di molecole in modo tale da poter comparare le diverse percentuali relative ai diversi campioni tra di loro. In questo caso, visto che la sansa di oliva è un materiale lignocellulosico, sono state scelte molecole in grado di rispecchiare il contenuto lignocellulosico dei 4 campioni: molecole aromatiche, alifatiche, contenenti gruppi carbossile e carboidrati. Essi infatti possono eventualmente essere presenti nei campioni ed essere associate in modo univoco a lignina, cellulosa o emicellulosa. Ognuna delle classi di molecole indagate hanno un picco che può essere usato per la loro identificazione: il gruppo carbossile ha un massimo attorno a 173 ppm; i gruppi aromatici hanno un massimo attorno a 154 (se presentano un atomo di ossigeno), 144 (aromatici legati l'uno all'altro), 129-116 ppm (aromatici sostituiti con una catena alifatica o non sostituiti), i carboidrati hanno un massimo attorno a 104 ppm, 72 ppm, 64 ppm, 56 ppm, gli alifatici (CH_n con n=1-3) non hanno un massimo, ma un'area tra 45 e 3 ppm. Per questa analisi sono stati scelti ^1H e ^{13}C come nuclei, ed è stata effettuata in un Bruker Avance DSX NMR spettrometro con un magnete da 9.4 T (frequenze di Larmor: 400.24 MHz per ^1H, 100.64 MHz per ^{13}C).

Un altro fondamentale parametro per la comparazione tra i differenti fuel solidi è il potere calorifico, che dà immediatamente un'idea sul contenuto energetico disponibile per essere sfruttato. L'analisi è stata effettuata in una bomba calorimetrica ad ossigeno Parr.

Come ultimo parametro scelto vi è la densità in cumulo, informazione che può rivelarsi necessaria nel design di un'apparecchiatura o nell'organizzazione dello stoccaggio di un materiale I valori determinati in questo lavoro fanno riferimento a una densità in cumulo con vibrazioni e senza.

Per quanto riguarda l'analisi di esplodibilità ed infiammabilità dei campioni, la prima analisi effettuata è stata per determinare l'energia minima di ignizione. Quando una polvere è dispersa in aria formando una nube, può potenzialmente essere innescata da una scintilla elettrica, derivante da un accumulo di elettricità elettrostatica, da un interruttore o da una scarica dovuta ad un'apparecchiatura particolare. Per quantificare il pericolo legato a queste situazioni, è possibile determinare l'energia minima che una scintilla elettrica deve avere per innescare la nube. L'apparato usato è un MIKE 3 (Fig. 2.2a) e la procedura standard seguita è l'ASTM E2019-03. Il volume del tubo di vetro è di 1.2 L, la dispersione della polvere avviene dal basso e l'energia della scintilla studiabile può essere variata da 1 a 1000 mJ.

La temperatura minima di auto-ignizione rappresenta la temperatura al di sotto della quale una nube di polvere non viene innescata da una superficie calda. La determinazione della MAIT infatti è stata effettuata in un BAM Oven da 0.35 L (Fig. 2.2b-c) secondo la procedura standard ASTM E1419-06. Questo apparato è fornito di una superficie parabolica al suo interno, sulla quale la polvere viene dispersa ed eventualmente si innesca. Se si innesca, tuttavia, la fiamma deve uscire dal flap entro 5 secondi, altrimenti il test è considerato negativo.

La concentrazione minima esplodibile (MEC) è la concentrazione minima alla quale un sistema polvere-gas può esplodere. È possibile determinare anche una massima concentrazione esplodibile, ma risulta troppo dipendente dall'apparato di misura e non potrebbe quindi essere usato come parametro di dimensionamento [10]. In questo lavoro, è stato usato una camera Siwek 20L (Fig. 2.3): la camera di esplosione è una sfera vuota di acciaio inossidabile, alla quale sono connessi un contenitore per la polvere e gli inneschi (è stato usato un innesco chimico da 2.5 kJ). La polvere è inserita nel contenitore, trasportata da un getto di aria compressa a 21 bar e dispersa da un ugello a farfalla (Fig. 2.4a-b). La misurazione è stata effettuata seguendo la procedura standard ASTM E1515-07.

Le esplosioni di polveri possono essere caratterizzate, oltre che dalla concentrazione minima esplodibile, anche dal relativo profilo pressione-tempo (come mostrato in Fig. 2.5), dal quale si possono dedurre importanti parametri come K_{St} e P_{max}. Il primo corrisponde alla velocità massima di aumento della pressione durante l'esplosione, mentre il secondo corrisponde alla massima pressione (relativa) raggiunta durante l'esplosione. In prima approssimazione, K_{St} permette di valutare i risultati di un'esplosione indipendentemente dall'apparato usato:

$$K_{St} = (dP/dt)_{max} * V^{1/3}$$

dove V è il volume della camera espresso in m^3, mentre P and t devono essere espresso in bar e s, rispettivamente. La misurazione è stata effettuata seguendo la procedura standard ASTM E1226-12a. secondo quest'ultima, ogni campione deve essere testato in due o tre serie (in questo caso, ogni serie va da 125/250 a 1250/1500 g/m^3, secondo il comportamento della polvere), e va assicurata la presenza di un massimo nella curva in funzione della concentrazione di polvere. Il software, poi, effettua la media aritmetica tra i massimi di ogni serie per valutare la P_{max} e il $(dP/dt)_{max}$ per ogni campione.

3. Risultati

I risultati dell'analisi della distribuzione granulometrica sono riportati in Fig. 3.1, mentre in Tabella 3.1 sono riportati I valori di D_{10}, D_{50} e D_{90} dei quattro campioni. Le curve sono tutte unimodali, ad eccezione del campione C, che mostra una piccola (e trascurabile) moda centrata a 18.5 µm. Le distribuzioni diventano sempre più strette man mano che la dimensione del campione decresce, mentre la percentuale di particelle fini cresce al decrescere della dimensione particellare del campione. Non ci sono gruppi isolate di particelle grossolane, che potrebbero influire pesantemente su esplodibilità e infiammabilità dei campioni [12], [13].

L'analisi termo-gravimetrica ha mostrato diversi comportamenti tra i campioni. Come si può notare in Fig. 3.2, la curva relativa al campione pellettizzato mostra qualche irregolarità in più rispetto alle altre curve. In ogni caso, tutte mostrano tre picchi riconducibili a ben noti fenomeni chimico-fisici [14], [15], [16], [17], [18]: il primo picco (ben visibile nel caso del pellet, quasi assente nel caso dei campioni polverizzati) è associabile alla disidratazione del campione; il secondo grande picco (all'incirca tra 180 e 370°C) è associato a reazioni di degradazione della materia lignocellulosica; il terzo (tra 370 e 520°C) è associato alla combustione del char, formatosi grazie alle reazioni avvenute precedentemente. Tutti gli step sono esotermici. Il campione D presenta un picco di combustione del char molto più alto degli altri, forse per l'elevata area superficiale ad esso associata.

Nella Tabella 3.2 sono riportati i risultati della proximate analysis: il campione B mostra la più alta reattività (VM/FC più alto), i campioni C e D sembrano avere reattività simile e il campione più grossolano (campione A) ha una reattività che è la più bassa. I risultati sono in linea con quelli di Miranda et al [20] (mostrati sempre in Tabella 3.2), che ha analizzato il comportamento termico di diversi residui derivanti da olive.

L'investigazione SEM si è rivelata utile per evidenziare diversità nella la forma delle particelle tra i campioni. Le immagini ottenute sono state riportate in Fig. 3.3. I campioni A e B mostrano una varietà di forme delle particelle, molto più degli altri due campioni, che sembrano avere particelle molto più uniformi nella forma, ma superfici meno lisce. Alcune strutture caratteristiche dell'oliva sono state identificate nei due campioni più grossolani (Tabella 3.3).

Per quanto riguarda il contenuto lignocellulosico dei quattro campioni, la solid-state NMR, i cui spettri sono riportati in Fig. 3.4 e 3.5, ha evidenziato come i contenuti delle molecole indagate siano pressoché uguali in tutti i campioni, con qualche differenza per il campione pellettizzato, come si può notare in Fig. 3.6. Gli spettri corrispondono all'intensità del segnale emesso dal detector in funzione del rapporto tra il chemical shift del nucleo considerato (^{1}H o ^{13}C in questo caso) e la frequenza del campo magnetico usata dal macchinario (moltiplicato tutto per un milione), così da ottenere un valore in ppm non legato ad alcun parametro dell'apparato.

I risultati della densità in cumulo (riportati in Tabella 3.4), mostrano come (prevedibilmente) in presenza di vibrazioni, la densità cresca. I valori sono tutti dello stesso ordine di grandezza. Tuttavia, i due campioni più fini presentano un aumento di densità in presenza di vibrazioni più accentuato rispetto agli altri due.

L'analisi dell'energia minima di ignizione ha portato alla conclusione che i quattro campioni non sono sensibili ad alcuna scintilla elettrica con un'energia associate minore di 1000 mJ (risultati mostrati in Tabella 3.5). L’analisi è stata effettuata (secondo la procedura standard ASTM E2019-03) usando diverse quantità di polvere (900, 1200, 1500, 1800, 2400 e 3000 mg), diversi delay time (90, 120 e 150 ms) e con induttanza (1 mH) per ogni campione, per prendere in considerazione ogni possibile scenario.

Lo studio della MAIT, i cui risultati sono riportati in Tabella 3.5, mostrano che i due campioni più fini sono più termicamente stabili degli altri due, visto che hanno una MAIT più elevata.

I risultati relativi ai parametri di esplosione sono riportati in Tabella 3.5. Il valore più elevato di P_{max} è relativo al campione B, mentre i campioni C e D mostrano valori abbastanza simili (sebbene una differenza di 0.3 bar non sia trascurabile parlando di P_{max}). Il campione più grossolano mostra il valore più basso. Per quanto riguarda $(dP/dt)_{max}$ (e quindi K_{St}) si nota un trend crescente al decrescere della dimensione particellare.

I valori di MEC determinati sono riportati Tabella 3.5. Essi sembrano seguire un trend decrescente al decrescere della dimensione particellare, andando dai 140 g/m^3 del campione più grossolano ai 90 g/m^3 del campione più fine.

4. Discussione

Dato che la sansa di oliva non è altro che il residuo solido proveniente dal processo di estrazione dell'olio dalle olive, è formata dai diversi tessuti che formano un'oliva: esocarpo (buccia), mesocarpo (polpa), endocarpo (nocciolo) e kernel (mandorla). Essi presentano diversi livelli di resistenza meccanica alla triturazione, quindi potrebbero mostrare comportamenti potenzialmente molto diversi nella fase di macinatura. Con la successiva setacciatura, si ottengono quindi frazioni con proprietà chimico-fisiche diverse. Infatti, Lammi et al [23], [26] hanno usato un sistema di frazionamento a secco facendo ricorso a soli trattamenti meccanici, per arrivare a separare una frazione ricca di polpa e una ricca di nocciolo. È quindi possibile assumere che triturazione e setacciatura hanno avuto un'importanza elevata sul comportamento dei campioni. Oltretutto, i risultati di ogni analisi sembrano aver confermato questa ipotesi.

Come è mostrato in Fig. 3.6, le percentuali delle molecole indagate non sembrano variare molto tra un campione ed un altro. Ciò significa quindi che il comportamento differente osservato durante i test di esplodibilità ed infiammabilità non è dovuto ad un cambio di composizione.

La causa principale potrebbe essere associata alle aree specifiche associate a differenti tipi di particelle. Infatti, se a_{Ti} rappresenta l'area superficiale totale del campione *i*, è vero che:

$$a_{Ti} = a_{buccia,i} + a_{polpa,i} + a_{nocciolo,i} + a_{mandorla,i}$$

dove $a_{buccia,i}$, $a_{polpa,i}$, $a_{nocciolo,i}$ e $a_{mandorla,i}$ sono rispettivamente le aree associate alle particelle provenienti dalla buccia, dalla polpa, dal nocciolo e dalla mandorla dell'oliva. Sebbene la loro composizione non cambia molto, le caratteristiche chimico-fisiche dei tessuti formanti l'oliva cambiano da uno all'altro. Questa potrebbe essere la ragione dei differenti comportamenti osservati.

Ciononostante, il contenuto ligno-cellulosico dei tessuti è difficilmente relazionabile a esplodibilità e infiammabilità dei campioni. Infatti, durante un'esplosione o un flash-fire, le reazioni di ossidazione, combustione e degradazione termica sono molto rapide e, come può essere notato in Fig. 4.2, all'aumentare della velocità di riscaldamento, le reazioni (rappresentate dai picchi) si sovrappongono l'un l'altra. Con una velocità di riscaldamento di 100 °C/min, che è comunque molto più bassa di quella raggiunta durante un'esplosione o un flash-fire, è stato individuato addirittura un solo picco. Pertanto, le analisi effettuate in questo lavoro non sono state sufficienti a trovare un legame tra la composizione dei campioni e le loro esplodibilità ed infiammabilità.

È conoscenza comune che le apparecchiature usate per i test di esplosione hanno una grande influenza sui risultati [30], [31], [32]. Ci sono molti parametri che influenzano esplodibilità ed infiammabilità di una polvere; quelli presi in considerazione in questo lavoro sono le modificazioni della distribuzione granulometrica dovute alla dispersione della polvere e la dipendenza del grado di mixing polvere-aria dal sistema di dispersione e dalla concentrazione della polvere. In ogni caso, tutti I parametri che influiscono sui risultati sono dovuti al fatto che in un sistema polvere-aria è molto difficile raggiungere un buon livello di mixing, proprio per la disomogeneità intrinseca di questo sistema, come sottolinea Chawla et al [30] nel suo lavoro.

In primis, è stato provato che la distribuzione granulometrica di una polvere dispersa nella camera di esplosione subisce una modifica (anche significative), dovuta alle interazioni interparticellari e particella-apparecchiatura. Bagaria et al [33], [34], tramite uno studio con sfere di 20 L, 36 L e 1 m^3, hanno concluso che una polvere può vedere modificata la propria distribuzione granulometrica anche del 78% (in termini di D_{50}). Questo valore sembra dipendere dall'indice di fragilità del materiale di cui è costituita la polvere: maggiore è l'indice di fragilità, maggiore sarà l'entità della modificazione della sua distribuzione granulometrica.

In secondo luogo, il sistema di dispersione sembra influenzare pesantemente il grado di mixing e la distribuzione della concentrazione nella camera. Di Sarli et al [35] hanno dimostrato, tramite la modellazione computazionale della dispersione di una polvere in una camera di 20 L di volume, che il rebound nozzle (lo stesso usato in questo lavoro) permette di iniettare quasi completamente tutta la polvere, non permettendo però di raggiungere un'omogenea distribuzione della concentrazione della polvere nella camera. Al contrario, il sistema anulare perforato permette di raggiungere una buona omogeneità della polvere nella camera, ma parte della polvere rimane nella sezione anulare, non venendo iniettata nella camera.

Infine, Di Sarli et al [36] hanno mostrato come anche la concentrazione di polvere (e quindi la quantità di polvere inserita nel dust-container) influenzi l'omogeneità nella camera. Sembra infatti che a basse concentrazioni (100 g/m^3) appaiano delle aree ad alta concentrazione attorno al vortice che si crea subito dopo la dispersione, ad alte concentrazioni (500 g/m^3) le aree ad alta concentrazione si spostano attorno al rebound nozzle (a causa di importanti fenomeni di sedimentazione), mentre a concentrazioni intermedia, l'omogeneità della concentrazione di polvere è massima. Detto questo, usando un range di concentrazioni non vicine tra loro è possibile stimare i parametri di esplosione con una buona accuratezza.

Un parametro di vitale importanza che va tenuto in considerazione è come viene fornita l'energia per l'innesco. Nella camera di esplosione l'innesco avviene grazie ad igniters chimici, che rilasciano innumerevoli scintille che accendono la nube. Nel BAM oven l'innesco è rappresentato dall'alta temperature della superficie parabolica all'interno della camera di combustione. Nel MIKE 3, l'innesco avviene grazie ad una scintilla elettrica. Ognuna di queste fonti di innesco sollecita la polvere in una maniera diversa dalle altre ed è una cosa da tenere in considerazione nella valutazione dei risultati. Inoltre, l'energia di ignizione sembra influire sui parametri di esplosione. È stato riscontrato che il campione C, per esempio, è stato molto influenzato dal variare dell'energia di ignizione (igniters da 2.5, 5 e 10 kJ), come mostrato in Fig. 4.3.

I parametri di esplosione e la MEC hanno mostrato come l'esplodibilità dei campioni è essenzialmente legata a due parametri: la composizione chimica (che influenza il contenuto energetico) e la distribuzione granulometrica (che influenza la velocità di propagazione di fiamma). Come atteso, $(dP/dt)_{max}$ (e anche K_{St}) presenta un trend crescente al decrescere della dimensione: 84 bar m/s (campione A), 166 bar m/s (campione B), 258 bar m/s (campione C) e 255 bar m/s (campione D). Invece, la P_{max} mostra un massimo: 7,3 bar (campione A), 8,4 bar (campione B), 7,8 bar (campione C) e 7,6 bar (campione D). Il trend della P_{max} è anche quello che presentavano HHV e VM/FC, indici del contenuto energetico che si libera effettivamente durante una combustione. Inoltre, in relazione ai valori di MEC, sembra che più il campione è fine e minore è il limite inferiore di esplodibilità, in linea con i risultati ottenuti da Semenova et al [37]. In conclusione, $(dP/dt)_{max}$,

K_{St} e MEC sono stati influenzati principalmente dalla dimensione delle particelle, mentre la P_{max} è stata influenzata dal contenuto energetico e dalla reattività chimica (VM/FC). In Fig. 4.3 sono riportati I risultati dei test di esplosione: sia $(dP/dt)_{max}$ che P_{max} sono riportati in funzione della concentrazione di polvere.

L'analisi per quantificare l'infiammabilità di una nube di polvere di sansa di oliva è stata lo studio della MIT, effettuata nel BAM oven. In esso, la nube colpisce una superficie parabolica riscaldata ed eventualmente viene innescata. In Fig. 4.4 sono riportate tutte le temperature testate. È stato osservato come, a temperature maggiori di 510°C, i due campioni grossolani (A e B) mostravano un'accensione immediate, classificabile come flash-fire. Al contrario, quando la temperatura era attorno ai 500°C o meno, la fiamma uscente dal fornetto era meno intensa e più lenta. Per quanto riguarda i due campioni più fini (C e D), la fiamma non è mai stata istantanea, ma probabilmente causata dall'accensione dei gas emessi dalla polvere. I risultati ottenuti sembrano in linea con i risultati ottenuti in altri lavori [39].

5. Conclusioni

Il pericolo associato alla manipolazione della sansa di oliva e alla potenziale formazione di polvere di sansa di oliva è stato studiato quantificando l'esplodibilità e l'infiammabilità quando dispersa in aria, per formare una nube. La dimensione particellare sembra non avere un ruolo da protagonista nel determinare I parametri di esplosione, ma piuttosto sembra che li governi insieme alla natura eterogenea del campione.

Il campione B ha mostrato in tutte le analisi il più alto contenuto energetico (HHV = 24.4 MJ/kg) e la più alta reattività termica (VM/FC = 11.8), il che porta ad ottenere la P_{max} più elevata (8.4 barg). I campioni C e D hanno mostrato un più basso contenuto energetico (rispettivamente, HHV = 23.7 e 22.6 MJ/kg) e una più bassa reattività termica (VM/FC = 5.7 e 4.4, rispettivamente), ma il più alto K_{St} (rispettivamente, 70 e 69 bar m/s). Il campione A ha mostrato un basso contenuto energetico (HHV = 22.9 MJ/kg) ma anche la più bassa reattività termica (VM/FC = 2.3), addirittura minore di quella del pellet; per quanto riguarda l'esplodibilità, questo campione ha mostrato la più bassa P_{max} (7.3 barg) e il più basso K_{St} (23 bar m/s). Sembrerebbe che la fase di macinatura e vagliatura abbia influenzato il comportamento dei campioni.

Il fattore più influente sulla Minimum Explosible Concentration è stata la dimensione particellare. Dato che né P_{max} né $(dP/dt)_{max})$) sono prese in considerazione per valutare la MEC, solo la dimensione particellare la influenza. I valori variano da 90 (campione D) a 140 g/m^3 (campione A).

Le nubi di polvere di sansa di oliva sembrano piuttosto sensibili all'auto-ignizione (causando flash-fire) quando esposte ad alte temperature, in particolare a superfici calde. I campioni hanno mostrato MAIT di 480 (campione B), 500 (campione A), 540 (campione C) e 550°C (campione D). Questi risultati sono coerenti con i valori di VM/FC, che quantificano la reattività termica dei campioni.

I campioni non sono risultati sensibili ad essere accesi da una scintilla elettrica con un'energia associata minore di 1000 mJ.

Dal confronto con il lavoro di Silva Durán et al [38], che ha preso in esame lo stesso campione di sansa di oliva, ma senza essiccarlo, sembrerebbe che con il 5-6%wt di umidità in più nel campione si arriva ad una riduzione del quasi 20% della P_{max}, mentre il K_{St} non sembra risentire di ciò (confronto dei risultati in Tabella 4.1). per quanto riguarda la MAIT, un interessante trend comune è stato osservato, sebbene le apparecchiature usate sono state differenti.

Questo lavoro potrebbe essere integrato con ulteriori informazioni, per ottenere una visione d'insieme del problema e comprendere più profondamente e dettagliatamente quali fattori concorrono a determinare i comportamenti osservati. Il primo fattore è la dimensione particellare, quindi lo studio di altri tre/quattro campioni con differenti diametri particellari (per esempio 100, 150, 250 e 500 µm) per ottenere dei trend più accurate e precisi. Un altro importante fattore è sembrato essere la fase di macinatura/vagliatura, perciò uno studio completo sui differenti sistemi di triturazione potrebbe illuminare sulle conseguenze sui campioni. Infine, un frazionamento a secco per ottenere una frazione ricca in polpa e una ricca in nocciolo consentirebbe di comprendere più a fondo l'influenza della natura eterogenea di questo tipo di campione.

1. Introduction

It is a fact and common knowledge that the Mediterranean Sea is a rich region and adapted to the growth of several vegetal species, as well as the production of a lot of products deriving from those. Among the typical activities in this region, there is the olive trees cultivation, from which it is possible to obtain numerous olive oil and olive qualities. The Mediterranean zone is responsible for the production of about 98% of the olive oil world-wide produced, which counts 900 million of olive trees occupying 10 million of hectares [1]. Furthermore, from each 100 kg of olive it is possible to produce about 60 kg of olive oil [1], which makes its production an important economic, cultural and political resource, especially for the countries which look out on the Mediterranean Sea. However, the manipulation of 100 kg of olives for the olive oil production is inherently bounded to the production of 40 kg of waste [1], which could represent a not derisory cost for an enterprise. It is in this area that can come into play a valorization system, which may transform these biomass wastes into a precious resource.

The by-products related to the olive oil production are principally 3: branches and leaves fallen in the olives harvest net and separated before the olive pressing; the watery effluent coming from the olives washing and from the use of water in the extraction process; the solid residue obtained after the decantation/centrifugation step, made predominantly of olive skin, pit and pulp. This last by-product is called olive pomace, nowadays used as animal feeding, soil improver, source of oil in the solvent extraction processes (to obtain pomace oil) and solid fuel for dust-burner, in order to get thermic energy [2]. Nevertheless, several other projects exist to employ olive pomace in different sectors: realization of construction material [3], biodiesel production [4], removing of the phenolic content in the olive mill wastewater [5], colorants absorption [6] and many others. In any case, its use as fuel in gasification, pyrolysis or combustion plants seems the most promising one nowadays and in the next future, especially because of the increasing energy world-wide demand and the consequent research of new energy resources. In fact, around the

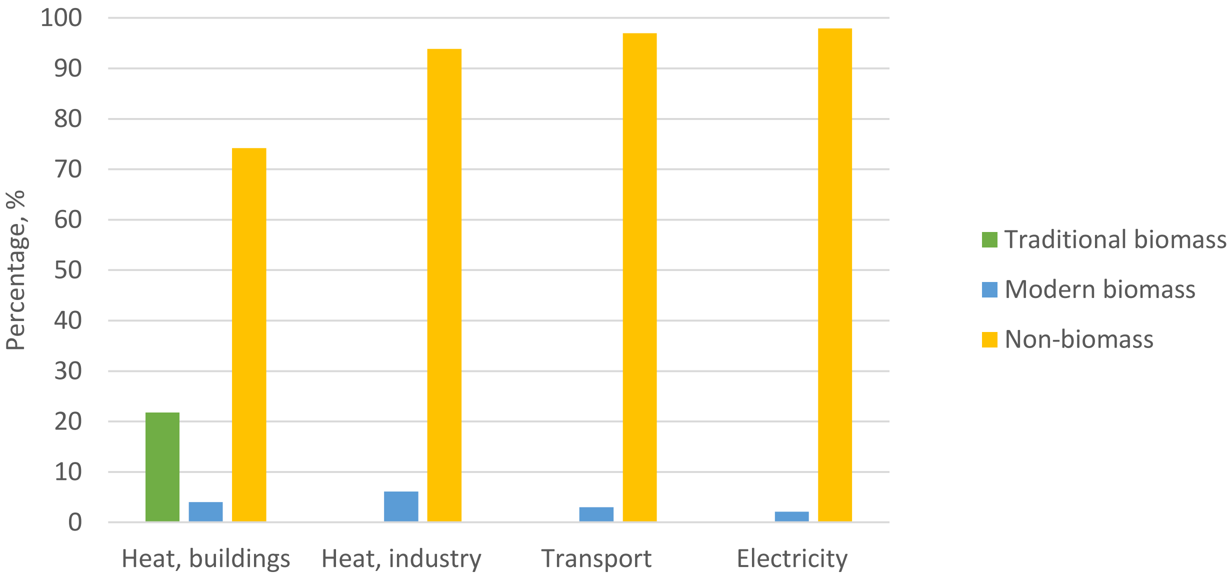

Figure 1.1 - Sources of the energy production in four different sectors in 2016: only the 12.8% came from the exploitation of biomass, and, besides, only a little part came from modern biomass (a biomass produced in a sustainable way). Data from [7].

turn of the XX century, the increasing need to reduce the negative impacts of fossil fuels on the environment has led humankind to start investing time and money in the new energetic resources research with fewer consequences on the Earth ecosystem and to the development of new exploiting technologies. Among these last, the exploitation of biomasses for energy purposes is very important, especially thinking about the biomass wastes. These can transform from a disposal cost an enterprise has to bear to an income it may obtain by their valorization. According to the Global Status Report 2018 of REN21 (Renewable Energy Policy Network for the 21st Century) although the energy production coming from the exploitation of a biomass in 2016 was only 12,8% against the 87,2% of non-biomass-deriving energy (see Fig. 1.1), the trend occurred between 2007 and 2017 shows clearly the increasing importance of the biomass in the energy domain. Furthermore, the world power production from biomass (traditional and modern ones together) moved from less than 250 TWh to more than 550 TWh in 2017, thus with an increasing of about 241% [7].

However, a direct consequence of the bioenergy production is the related industrial hazard increase. In fact, as can be seen in Fig. 1.2, the number of incidents (normalized according to the net produced energy) from the biennium 1996-98 to the 2011-2013 one has increased almost 7 times [8], considering solely the energy produced from biomass, and more than 4 times considering the energy produced also from biofuels and biogas (indicated as bioenergy in Fig. 1.2). Plus, it is exactly the biomass area the origin of the majority of the incidents in the bioenergy domain. It can be concluded that a study of the eventual and possible energetic valorization of a biomass is not enough for it to be introduced in an industrial reality, but it is necessary to study the hazard related to its employment and handling. For this very reason, the potential and increasing use of olive pomace in the industrial domain must include a study of the hazard related to its handling.

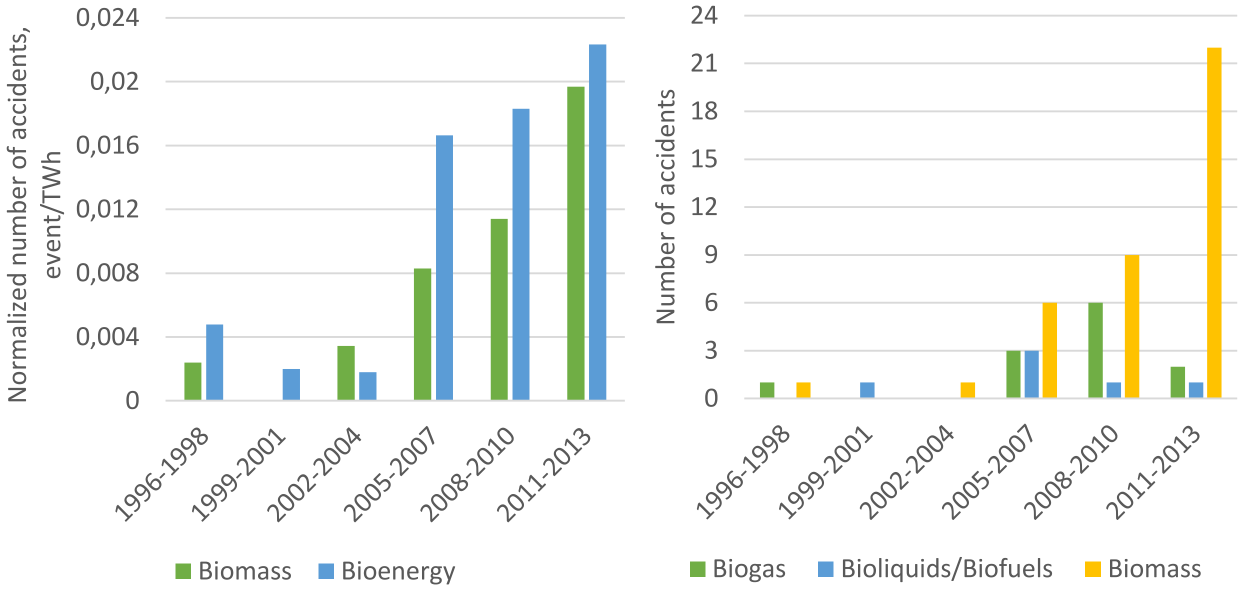

Figure 1.2 - On the left, the number of accidents in bioenergy production plants (normalized by the electricity net generation) over the years, with the comparison between biomass-sourced energy and bioenergy itself. On the right, number of accidents in bioenergy domain, with specification of which type of used bio-source. Data from [8].

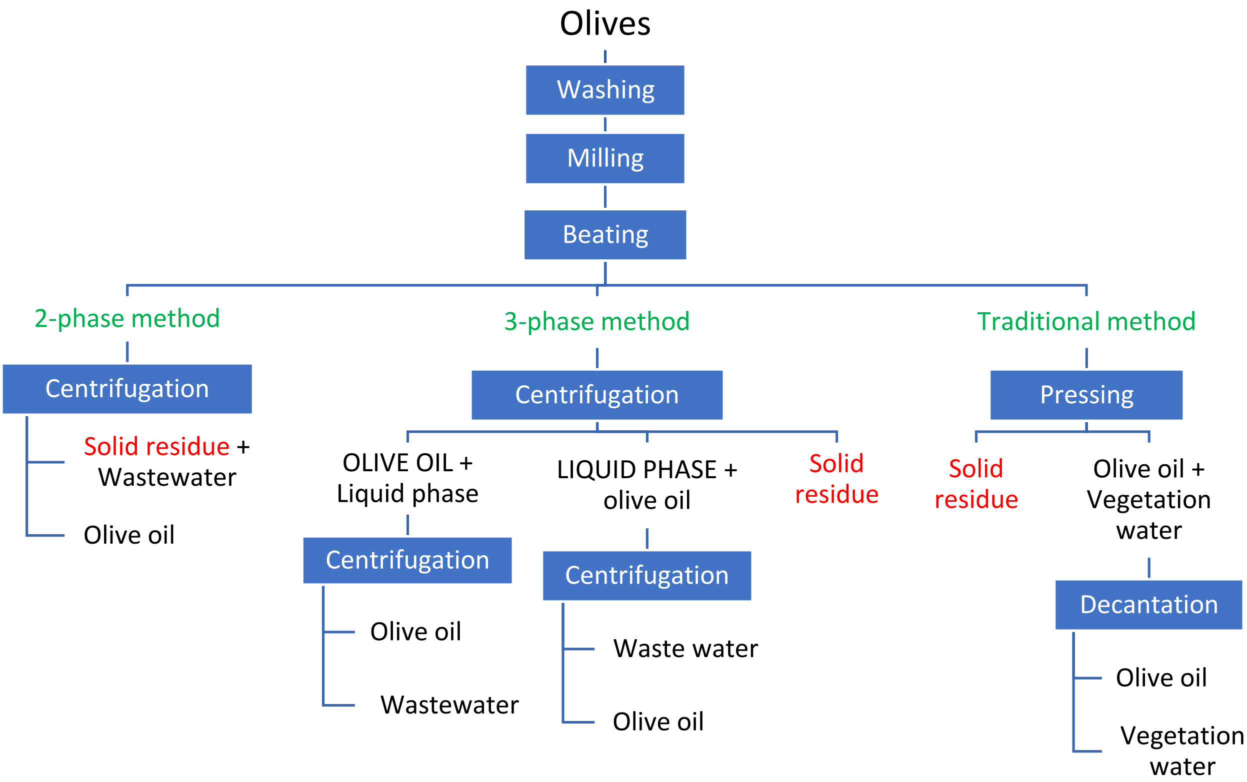

Figure 1.3 - Olive oil production methods. In red, the position of olive oil solid residue (olive pomace) in the flowchart of olive oil production processes. From [9].

Olive pomace can be found in different industrial realities: silos stocking (with the potential formation of fines), gasification and pyrolysis in reactors (with potential formation of dust clouds in a high temperature environment), undesirable deposits in milling and/or grounding systems (with potential contact with hot surfaces). These situations are only a few of those possibly present in an industrial reality and they can lead to fire and/or explosion, with severe consequences on systems, on people working in situ or just in the area around. Furthermore, literature lacks in information about olive pomace, and it lacks even more speaking of hazard related to its handling.

The present work aims to elaborate a risk assessment analysis, focused on explosibility and flammability of olive pomace dust, on the comprehension of its behavior in the above-mentioned situations and on the identification of the worst scenarios involving olive pomace dust.

To understand completely its characteristics of explosibility and flammability, it is fundamental to know the different olive pomace production processes. First, the olive oil extraction can occur in three different ways, as presented in Fig. 1.3: traditional process, 2-phase or 3-phase process [9]. In the first case, after the olives milling, the paste is rested in order to obtain a natural decantation of the mass and the natural separation of olive oil from the solid phase. With the 2-phase and 3-phase processes, instead, to increase the productivity, a centrifugation step is placed right after the milling. It is in the 3-phase process that in this step there is a water injection. Thanks to a pure mechanical action of the water, the separation is better and thus the extracted olive oil amount is bigger. At the end, in the 3-phase process, there are 3 phases obtained (aqueous, oily and solid). In any case, at the end of the extraction, a slurry olive pomace is obtained. Then, it is dried and sent to its destiny. Its manipulation and handling can be facilitated through a light grinding, to obtain chunks with an average diameter of 5-10 cm, or through a deeper trituration, to obtain a powder with an average particle size of 1 mm, which is then pelletized. In this work, the olive pomace analyzed (Figure 2.1a) comes from Spain, from an olive-mill that uses a 2-phase method as extraction method, with a final pelletizing step. Since the pelletized form does not pose any hazard more than a woody material pile, the olive pomace explosibility and flammability hazard analysis is focused on its pulverized form, the most dangerous form that can be found in the industrial reality.

This study was carried out analyzing the behavior of 4 different samples, coming from the same olive pomace, but with different particle size. The choice of the 4 particle sizes is due to the need to obtain information in a quite wide range: 400 µm to represent coarse particles, 200 µm to represent intermediate particles, 80 and 45 µm for the fines. The lower the particle size, the higher the probability for different phenomena (cohesion forces, agglomerates formation, important heating in the grounding step). Therefore, two particle sizes were chosen to represent the fines.

In order to know their nature, a chemical-physical characterization was made on the four samples, plus some on the pelletized one, by determining:

- The moisture content
- The particle size distribution
- The shape and the outlook of the particles, through a SEM investigation (Scanning Electronic Microscope)
- The thermal behavior, through a thermo-gravimetric analysis
- The chemical composition, through a solid-state ^{1}H-NMR (^{1}H-Nuclear Magnetic Resonance)
- The calorific value
- The bulk density

As regards the risk assessment analysis, several analyses were carried out to determine the following characteristics of the samples:

- Minimum Auto Ignition Temperature (MAIT)
- Minimum Ignition Energy (MIE)
- Minimum Explosible Concentration (MEC)
- Explosion parameters (P_{max}, $(dP/dt)_{max}$ and K_{St})

2. Material and analyzes

2.1 Characterization analyzes

2.1.1 Sample preparation

The sample in its pelletized form was ground in a TM hammer mill, then sieved with a Model B Ro-Tap test sieving shaker, in order to obtain the wanted samples. The choice of the particle sizes was made also according to the availability of sieves; thus, the chosen ones were 425, 212, 75 and 45 µm. Hence, the obtained fractions were the one between the 425 and 212 µm sieves, between the 212 and 75 µm sieves, between the 75 and 45 µm sieves and the one passed through the 45 µm sieve. From now on, they are going to be referred, respectively, as sample A, B, C and D. After these steps, samples were dried in an air-oven at 110°C for 24 h to achieve a moisture content lower than 5%wt. In Fig. 4, the four samples after the preparation part are shown.

2.1.2 Moisture content

Knowing the sample moisture content is essential, because the too wet sample may necessitate of a drying step. In fact, according to the E1226-12a, performing tests on a sample with a moisture content higher than 5%wt may lead to results strongly influenced by the presence of water. On the other hand, if the moisture content is lower than 5%wt, the water influence on explosion parameters is negligible.

The determination of the moisture content was made with a Sartorius Moisture Meter MA and measurements were repeated three times for accuracy and precision reasons.

2.1.3 Particle size

The particle size distribution is another characteristic that must be considered. Since the majority of the powders is formed by different sized and different shaped particles [10], it is necessary to approach the particle size distribution in a statistical way. Two types of graphs can be obtained: a frequency distribution and a cumulative distribution. In the first case, the fraction of particles having a diameter in a certain diameter range is reported in function of the diameter range. In the second case, data are the same, but the particle fractions are added with those relative to lower diameters, obtaining an increasing particle fraction (until 100%). In both cases, a discrete distribution is obtained, that can be converted in a continuous distribution if the resolution degree is high enough.

Particle size distributions can greatly affect the dust behavior: the smaller the particle size, the higher the surface area available, thus higher the reactivity. However, smaller the particle size, higher the probability of the appearance of secondary phenomena (cohesion forces, agglomerates formation and other phenomena linked to the nature of the dust).

The analysis was performed with a Microtrac S3500, coupled to a Microtrac Turbotrac for the dust dispersion.

2.1.4 Morphology

The SEM investigation allows to describe the particle shape and the eventual presence of peculiar structures or agglomerates. Furthermore, the shape of particles is an important characteristic influencing the explosibility and the flammability of the dust. More distant their shape is to the spherical one, higher the surface area available for mass and heat transfer. Before using the microscope, particles must be coated to become electrically conductive.

The coating was made using a Low Vacuum Coater Leica EM ACE200 (current intensity of 20 mA, exposition time of 260 s, pressure of 0,04-0,08 bar). At the end, particles were coated with a 20 nm gold-palladium layer. The SEM investigation was carried out with a Hitachi S-4700 Field Emission Scanning Electron Microscope, using a potential of 10 kV.

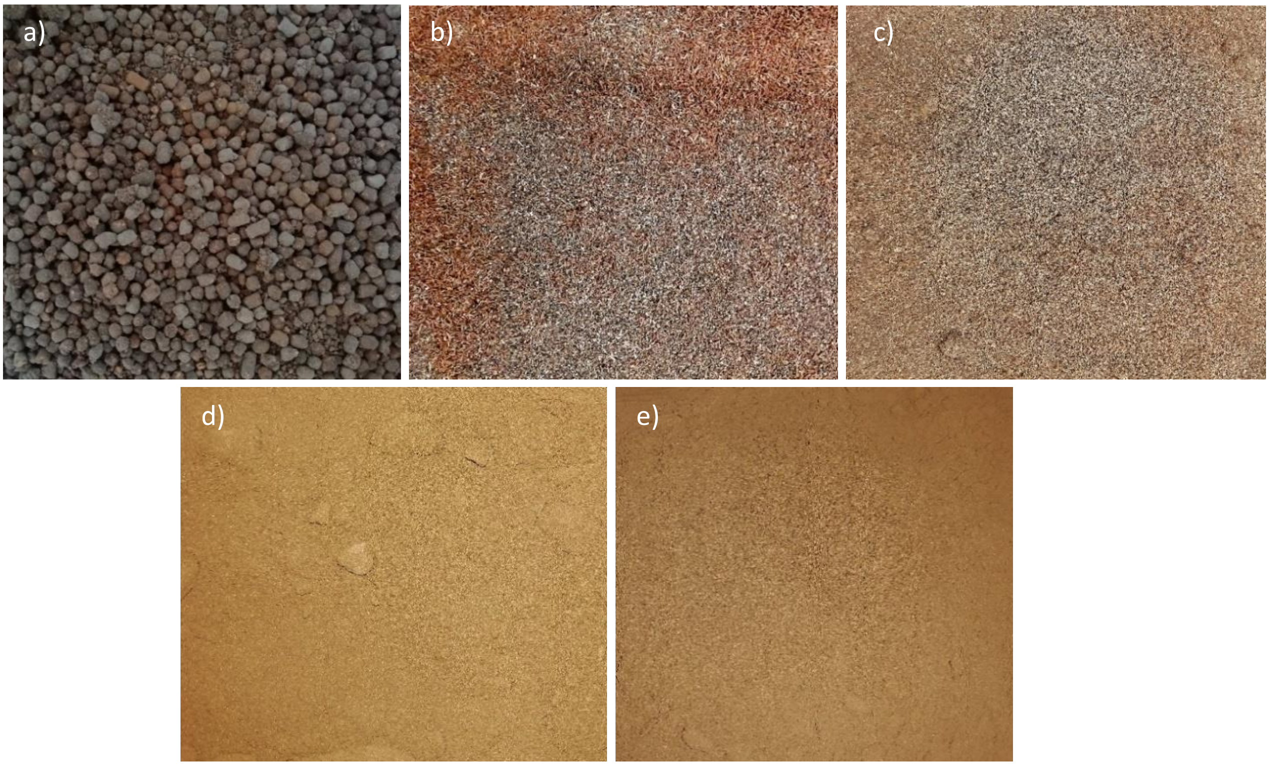

Figure 2.1 - The four olive pomace dust samples: a) pelletized form; b) sample A; c) sample B; d) sample C; e) sample

2.1.5 Thermal behavior

The thermo-gravimetric analysis (TGA) gives information about the thermal behavior of the sample (when it is heated steadily), particularly how the mass of the sample changes with the increasing of the temperature. And in so doing, mass losses associated to phenomena such as dehydration thermal degradation, oxidation reaction and so on, are highlighted. Having the results from both the under-air and under-nitrogen test, it is possible to determine the moisture content (MC), the volatile matter (VM), the fixed carbon (FC), the ash content of the sample, using the formulas reported in Table 2.1. VM is the matter capable of volatize (when the temperature is high enough) with or without an oxidizing atmosphere, while FC is the residue after the volatile matter is expelled. Both influence the combustion behavior and can be used as indicator of the biomass reactivity. In fact, high VM and low FC means higher reactivity of the biomass [19].

Table 2.1 - Formulas used for the proximate analysis. a Used only for the pellet sample, which was not subject to the moisture content analysis.

Moisture content [a]	$\frac{M_i - M_d}{M_i} * 100$
Volatile matter	$\frac{M_d' - Ash}{M_d'} * 100$
Fixed carbon	100 – MC – VM – ASH
Ash content	$\frac{Ash}{M_d} * 100$

where M_i is the initial mass, M_d and M_d' are respectively the mass at the end of the dehydration peak under air atmosphere and under inert atmosphere, Ash is the solid residue at 990°C. The analysis was performed in a Q600 SDT (Simultaneous Differential Technique), with a heating rate of 10°C/min, a final temperature of 1000°C, under air and argon atmosphere.

2.1.6 Chemical characterization

Through a solid-state NMR it is possible to obtain information about the sample's chemical composition, in terms of specific molecules class specifically chosen basing on the type of sample. In this case, knowing that the sample is a lingo-cellulosic matrix, the results may allow to estimate its chemical composition in terms of lignin, cellulose and hemicellulose contents, but moreover to notice an eventual change in the composition among the samples. Depending on the analyzed nuclei (^{1}H, ^{13}C, ^{15}N, etc.), results can be associated to a high- or low-resolution degree. For this analysis, ^{1}H and ^{13}C were chosen as nuclei. To enlighten the eventual different chemical character of the five samples (4 dusts and the pellet) 4 chemical classes were chosen, onto which carrying out the analysis: carbohydrates, aromatics, carboxylic and aliphatic species. Each of them has a specific maximum that can be used for the characterization: carboxyl groups have maxima around 173 ppm (integral range 191 - 164 ppm); aromatic groups (integral range 164 - 112 ppm) have maxima around 154 ppm (aromatic containing oxygen atoms), 144 ppm (aromatics bonded each other), 129-116 ppm (aliphatic-substituted or non-substituted aromatics); carbohydrates have maxima typically around 104 ppm, 72 ppm, 64 ppm, 56 ppm (integral range 112 - 45 ppm); aliphatic (CH_n where n=1-3) have not specific maxima (integral range 45 - 3 ppm).

This analysis was carried out in a Bruker Avance DSX NMR spectrometer with a 9.4 T magnet (Larmor frequencies: 400.24 MHz for ^{1}H, 100.64 MHz for ^{13}C) using a probe head for rotors of 4 mm diameter.

2.1.7 Calorific value

Calorific value is another parameter of fundamental importance speaking of biomass fuel: it allows to know the amount of thermal energy released by its complete combustion and thus the thermal energy potentially exploitable for energetic purpose. Furthermore, it allows to quickly compare two or more fuels among each other. Usually, the calorific value is determined with a calorimetric bomb, that measures the temperature increase of a precise amount of water to calculate the heat released during the sample combustion.

The analysis was made with the help of a Parr oxygen calorimetric bomb.

2.1.8 Bulk density

When a solid material is stocked, has been put inside a reactor or simply amassed somewhere, it is useful to know the bulk density, to estimate the occupied volume or the weight of a certain volume. It can be estimated for some static places (stocking, fixed bed) or for some moving/vibrant places (stocking with vibrations, sieves). In presence of vibrations, bulk density usually gets higher. The analysis was made by simply putting a known amount of powder in a graduated cylinder, then dividing the known mass by the measured volume. By tapping the cylinder until stabilization of the volume it was possible to estimate the bulk density in presence of vibrations.

2.2 Explosibility and flammability analyzes

2.2.1 Minimum Ignition Energy

When a dust is dispersed in a gaseous medium it can ignite only if a certain amount of energy is supplied. The minimum energy to supply to a dust cloud to have it ignited is the Minimum Ignition Energy (MIE). The provided energy may be in the form of a flame, a hot surface, a hot environment or a spark, but the MIE is usually referred to a spark. This last is an ignition source largely present in an industrial environment: electrostatic discharges from electrical equipment, the electrical sparks caused by switching operations, as well as the electrostatic sparks caused by process operations such as pouring [11]. To have an idea of the importance of sparks as ignition sources on olive pomace dust clouds a MIE analysis was made.

The apparatus that was used is a MIKE 3 (Fig. 2.2a), using a glass tube as explosion vessel and generally following the ASTM E2019-03 standard procedure. The glass tube has a volume of 1.2 L, the dispersion occurs with pressurized air (7 bar) and through a mushroom-shaped nozzle placed at the bottom of the tube. The analysis was carried out (according to the ASTM E2019-03 standard procedure) with different amounts of dust (900, 1200, 1500, 1800, 2400 and 3000 mg), different delay time (90, 120 and 150 ms) and with inductance (1 mH) for each sample, in order to study several potential situations. This system allows to vary the spark energy within the range 1-1000 mJ. The procedure provides for repeating 10 times the dispersion-spark step, in order to collect a statistically-valid number of results. The software takes account of the number of tests necessary to ignite (or to not ignite) the dust cloud in order to determine a statistical ignition energy (E_s), between the lowest energy at which the dust cloud ignites and the highest energy at which the dust cloud does not ignite.

The analysis on the four samples was carried out after a calibration step with Lycopodium and CaRo13 (see results in Appendix).

2.2.2 Minimum Auto Ignition Temperature

Also known simply as Minimum Ignition Temperature (MIT), it represents the minimum temperature at which a system (in this case a dust cloud) can ignite without the action of an ignition source, such as sparks or flames. For example, the ignition may occur due to the contact with a hot surface: a certain amount of thermal energy is transferred thus to the sample, allowing this last to achieve a temperature high enough for the ignition.

The MAIT measurement was made with a 0.35L BAM Oven (Fig. 2.2b-c) generally following the ASTM E1419-06 standard procedure. The apparatus consists of a furnace, heated by an electrical resistance, within which there is the ignition chamber, where the dust is dispersed. The injection of the sample is done through a manually-squeezed pump. Right after the injection, the dust cloud thus formed in the internal chamber hits a heated parabolic-shaped surface: if the temperature is high enough, there will be ignition and a flame will come out from a flap behind the surface; if not, no flame will come out of the apparatus. The ignition may take place in two ways: the first one is the direct ignition (the sample goes up to a temperature higher than the MAIT in the very moment of the contact with the hot surface), while the second one is the off-gases ignition (the sample settles inside the chamber and the off-gases, coming from thermal degradation reactions, ignite). In both cases, a test is considered positive if the ignition occurs within 5 seconds from the dust injection.

The analysis on the four samples was carried out after a calibration step with Lycopodium (see results in Appendix).

2.2.3 Minimum Explosible Concentration

The MEC is the minimum concentration at which a combustible dust-and-gas system can ignite and explode. When dust is in default compared to the oxygen, transfer phenomena between particles and combustion reactions occur with low rates, determining a not-well-sustained flame propagation. Below a certain limit (MEC), the flame propagation cannot be supported and, thus, there is no chance for the system to generate an explosion. As the MEC exists, also a Maximum Explosible Concentration does, and it is referred to the maximum concentration of dust in a gaseous medium capable of supporting a flame propagation. Beyond this point, the dust particles act as a heat sink and absorb any kind of heat released by any eventual reactions, determining an incapability of the system to sustain a flame propagation. However, this parameter has been found to be intimately related to the test apparatus design and the test procedure that, as consequence, has a low degree of reproducibility. For this reason, the Maximum Explosible Concentration is inappropriate for engineering design purposes [10].

For this work, a Siwek 20L vessel was used (Fig. 2.3): the explosion chamber is a stainless-steel hollow sphere, to which are connected the dust container (through the outlet valve) and the igniter (one 2.5 kJ chemical igniter was used as ignition source). The dust is inserted in the dust container, dispersed in the chamber by 21 bar compressed air and a rebound nozzle. It has been found that the dispersion system has an important influence on the explosion [12]: not only it must be calibrated in relation to the nature of the sample (agglomerates formation, fibrous sample, etc.), but also in relation to the delay time set for the explosion tests. Furthermore, it must allow to achieve a good degree of mixing between dust and air. In this case, a butterfly-shaped rebound nozzle was used (Fig. 2.4a-b). The test was considered positive (ignition of the dust cloud) if the P_m achieved at least 1 barg, otherwise the test was considered negative. The MEC was reached when two negative tests (two tests without ignition of the dust cloud) were obtained consecutively. The measurements were undertaken generally following ASTM E1515-07 standard procedure.

The analysis on the four samples was carried out after a calibration step with Lycopodium (see results in Appendix).

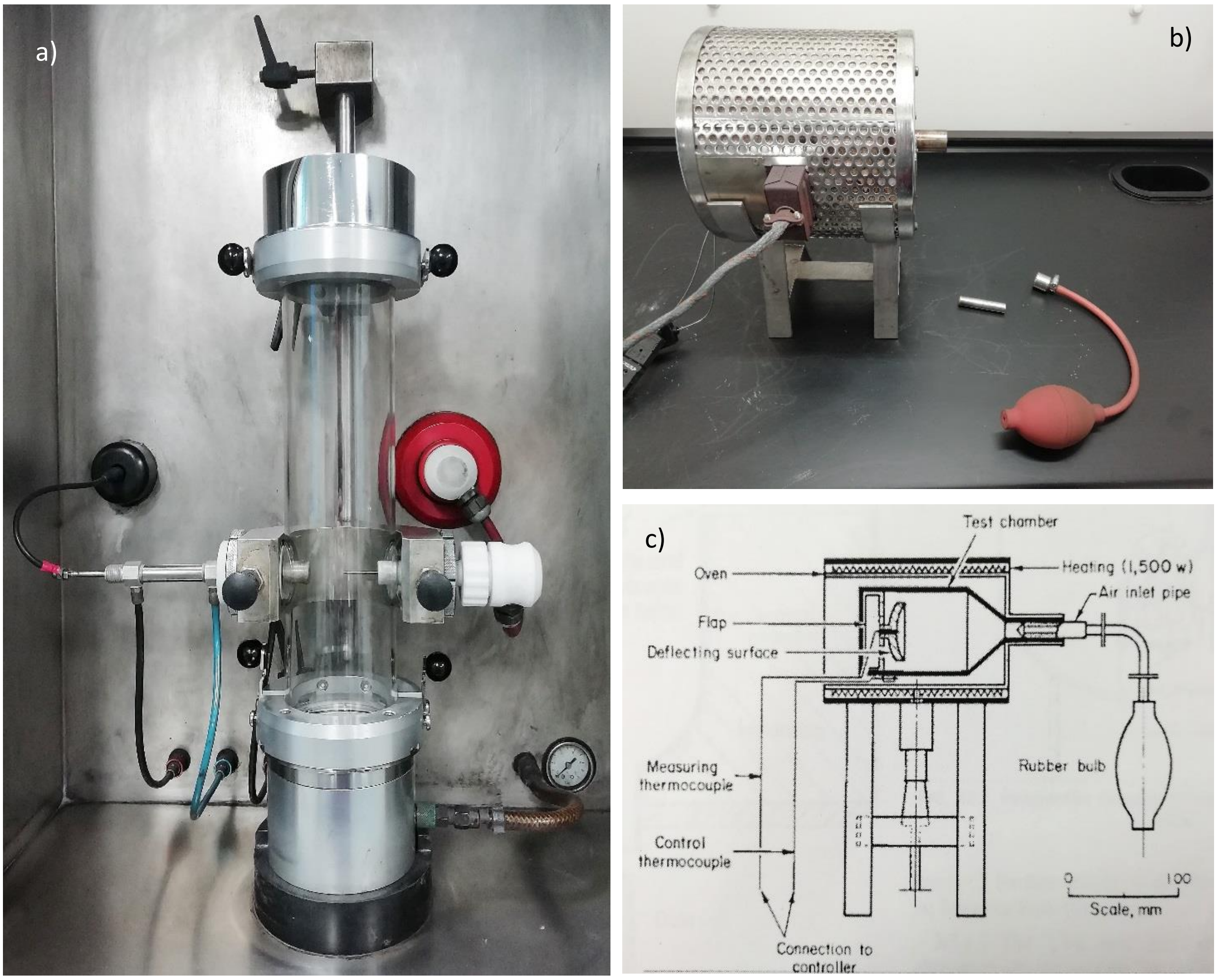

Figure 2.2 – a) MIKE 3 apparatus; b) BAM oven with rubber pump; c) BAM oven scheme section.

2.2.4 Explosion parameters

Dust explosibility can be characterized, other than by the MEC, by the associated pressure profile over the time, from which it is possible to deduce two important parameters: K_{St} and P_{max}. The first one corresponds to the maximum rate of pressure rise (the maximum slope of an explosion pressure profile, as shown in Fig. 8), while the second one to the maximum value of pressure achieved during the explosion. The K_{St} is related to the mass burning rate of the fuel, so it is intimately linked to the sample composition and particle size, as well as its concentration in the dust-air mixture [12]. Furthermore, it is very sensitive to the size and the shape of the test vessel [10], as they influence both the dust dispersion and the heat losses to the vessel wall. To a first approximation, K_{St} can be disjointed from the dimension of the spherical vessel where is measured in through a simple correlation:

$$K_{St} = (dP/dt)_{max} * V^{1/3} \quad (2.1)$$

where V is the volume of the vessel expressed in m^3, while P and t have to be expressed respectively in bar and s. P_{max}, on the other hand, is influenced by the energetic content of the dust but not by its particle size, which has an effect only on the heat release rate (then on the pressure rise rate) [12]. It is solely the maximum temperature (ideally, the adiabatic temperature) achieved during the explosion to determine the P_{max}.

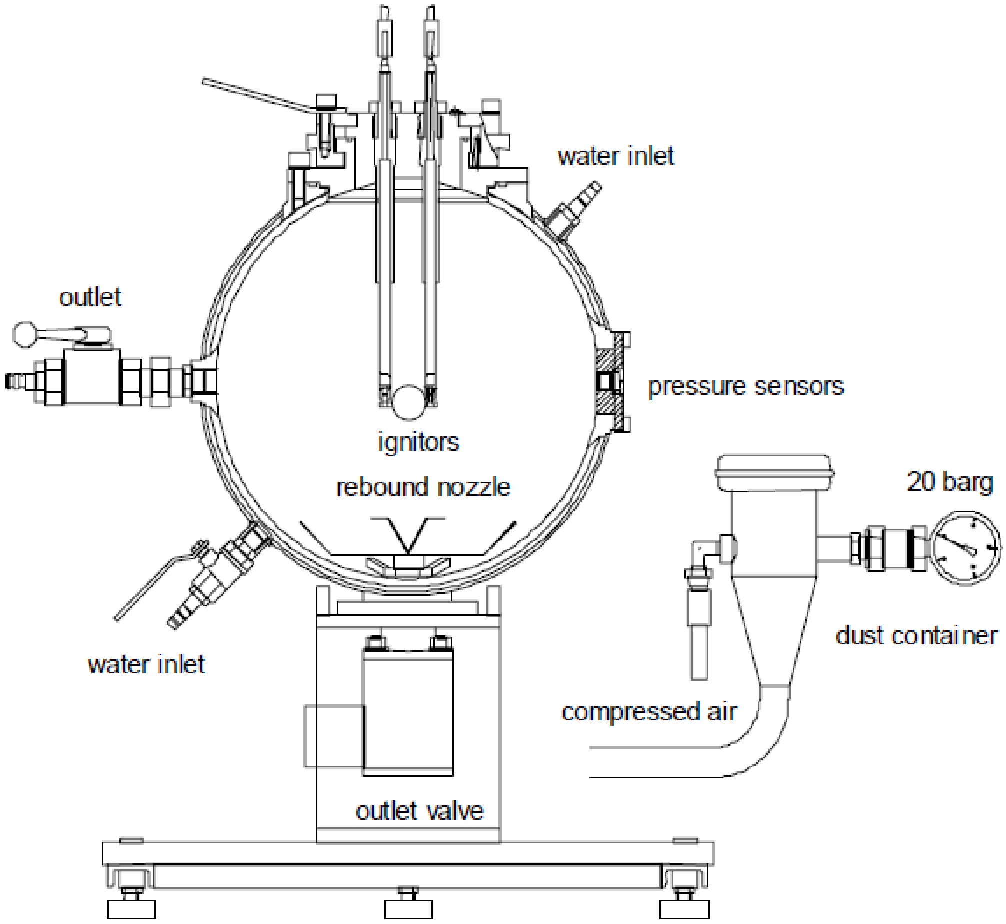

Figure 2.3 - 20L vessel system used for the explosion test.

The measurements were undertaken generally following ASTM E1226-12a standard procedure. This last provides for each sample to be tested over two or three series (in this case, each series goes from 125/250 to 1250/1500 g/m^3, depending on the dust behavior), in order to ensure the right position of P_{max} and $(dP/dt)_{max}$ in the studied concentration range. Each series must show a maximum value and a upside-down-parabolic trend to be considered helpful for the investigation. Once individuated the two-three series, the software considers the maximum values of each series and average them to calculate P_{max} and $(dP/dt)_{max}$. The software that was used for the measurements was the KSEP 6.0. It was able to record several quantities related to the explosion, as can be seen in Fig. 8, where a typical pressure-over-time profile is reported. In Table 2.2 are explained the quantities reported in Fig. 2.5. Before the explosion occurs, the chamber pressure is reduced to 0.4 bar (absolute), in order to purge the air inside and bring the pressure exactly to the 0-bar(g) line at the ignition time. Then, the dust is dispersed and ignited, causing the pressure rise. The explosion overpressure P_{ex} is affected by different phenomena: the dust ignition, the igniters opening and the cooling effects. First and foremost, the augmentation of the temperature caused by the ignition of the dust leads to a rapid increase of the pressure, but also igniters cause an increase of the temperature, even though with smaller magnitude than the dust. Cooling effects (through the vessel wall mainly), instead, tend to reduce P_{ex}. To carve out the effects not due to the dust explosion, two cases were identified: if the $P_{ex} \geq 5.5$ barg, the cooling effect is important (especially if it is desired a comparison between 20-L and 1-m^3 vessels), while the igniters contribute is negligible; if the $P_{ex} < 5.5$ bar, then the igniters contribute becomes important and the cooling effect negligible. One expression is associated to each of the explained two cases:

$$P_{ex} \geq 5.5\ \text{barg} \rightarrow \qquad P_{ex} = 0.775 * P_{ex}^{\ 1.15}$$

$$P_{ex} < 5.5\ \text{barg} \rightarrow \quad P_{ex} = \frac{5.5 * (P_{ex} - P_{ci})}{(5.5 - P_{ci})} \quad , \quad P_{ci} = 1.6 * \frac{IE}{10000}$$

where P_{ci} is the pressure due to the chemical igniters and IE is their energy. All pressure values must be expressed in barg. Another important parameter is t_v, the time interval in which the dust dispersion takes place. It has to be chosen carefully: if it is too high, the dust will tend to deposit,

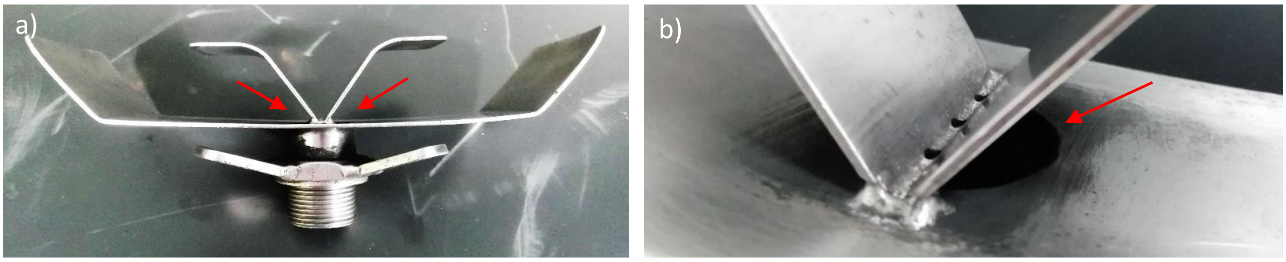

Figure 2.4 - Butterfly-shaped dispersion device used during the explosion tests (a). The suspended-dust flow enters from the bottom (ridged-edge part) and flows through the two big holes (indicated by the arrows) under the small wing in the center, to be then deflected by the two big external wings. Three tiny holes (b) allows the dust also to occupy the central part of the chamber, to have an even higher mixing degree.

while if it is too low, the dispersion degree will not be high to ensure a good homogeneity of the dust concentration. In this work a t_v = 60 ms was chosen.

The analysis on the four samples was carried out after a calibration step with Lycopodium (see results in Appendix).

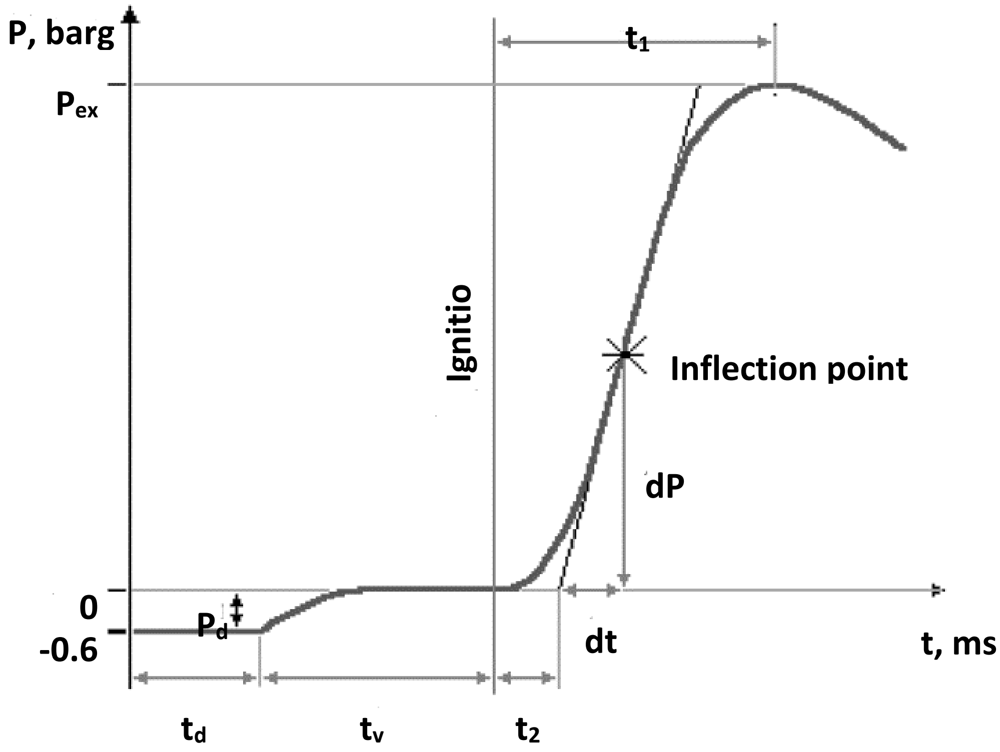

Figure 2.5 - Example of a typical pressure-time profile.

Table 2.2 - Parameters measured or calculated by the software used in the explosion tests.

Symbol	Quantity	Definition
P_{ex}	Explosion overpressure	Difference between the pressure at the ignition moment and the maximum pressure achieved during the explosion. This is relative to one single test.
P_m	Corrected explosion overpressure	Corrected P_{ex}, due to cooling effects and the pressure contribution of the igniters. This is relative to one single test.
P_{max}	Maximum explosion overpressure	Maximum value of Pm calculated over a series of tests carried out with different dust concentrations.
$(dP/dt)_m$	Rate of pressure rise	Maximum slope of a tangent to the P-t profile (tangent to the inflexion point). This is relative to one single test.
$(dP/dt)_{max}$	Maximum rate of pressure rise	Maximum value of $(dP/dt)_m$ calculated over a series of tests carried out with different dust concentrations.
K_{St}	Explosibility index	Defined by Equation 2.1. It allows to compare explosion behaviors obtained from different explosion vessels (20-L and 1-m^3, for example)
P_d	Expansion overpressure	Difference between the pre-vacuum and pre-ignition pressure. The standard value is 0.6 barg.
t_d	Time-delay of the outlet valve	Time between the activation of outlet valve and beginning of the pressure rise. This time-delay must be in the range of 30 to 50 ms.
t_v	Ignition delay time	Time between the dust dispersion and the ignition moment.
t_1	Duration of combustion	Time between the ignition moment and the culmination point, when the P_{ex} is achieved.
t_2	Induction time	Time between the ignition moment and the intersection of the inflexion-point tangent with the 0-bar line.

3. Results

3.1 Characterization analyzes results

3.1.1 Particle size

It is impossible with only a grinding step to know a priori the particle size distribution, whether it is unimodal, bimodal or the mean value is too high or too low than wanted. For this reason, after the samples were ground, several trials of sieving were done, according to the particle size distribution that each time was obtained. For samples C and D, distributions were well centered around the wanted value right after the first sieving, thus there was no need to proceed further with the sieving. In the case of samples A and B, instead, one further sieving step was done, in order to obtain respectively a unimodal distribution and a narrower distribution and centered around 425 µm. The final granulometric distributions are shown in Fig. 3.1. Table 3.1 shows samples D_{10}, D_{50} and D_{90} values. Distributions are all unimodal, except for sample C, which shows a little (and negligible) mode centered in 18.5 µm. It can be seen how the distributions get narrower and narrower as the particle size decreases. For example, for sample A, the difference between D_{90} and D_{10} is 454 µm, while that of the sample D is only 42 µm. That means the percentage of fine particles get in turn higher and higher as the particle size decrease. Furthermore, there are no isolated groups of coarse particles (as it happens in a bimodal distribution with one of the mode-values in the coarse particles range), which act like a heat sink during the explosion. In fact, Saeed et al [12] concluded that in rice husk dust explosion, are the fine particles to propagate the flame throughout the dust cloud, while the coarse ones burn behind the flame front. Plus, the model proposed by Andrews et al [13] seems to confirm that theory: the explosion-induced wind acts separating the coarse to the fine particles, according to their weight, ending up with the fines propagating the flame front and the coarse behind it and burning in the burnt-gases zone.

Table 3.1 - D10, D50 and D90 values for the four samples.

SAMPLE	D_{10}	D_{50}	D_{90}
A	162	388	616
B	43	162	255
C	19	63	104
D	10	30	52

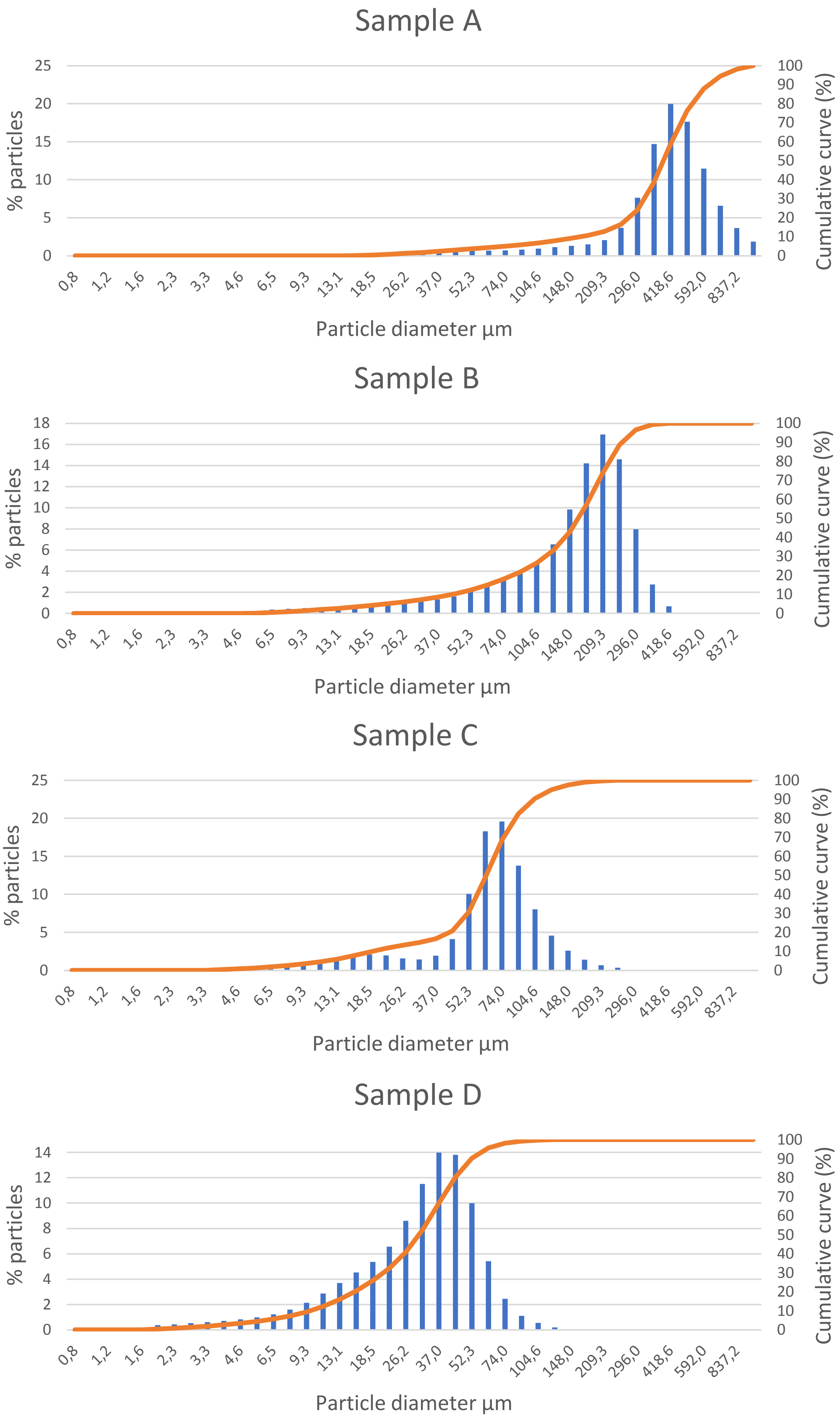

Figure 3.1 – Particle size distribution of the four samples. From the top: sample A, B, C and D.

3.1.2 Thermal behavior

The TG analysis showed the samples had different behavior when heated up. As it can be seen in Fig. 3.2, the pellet curve shows some irregularity compared to the others: the first wide peak is associated to the loss of the free and bounded water (the other four samples do not show such a peak because they passed through an air-oven-drying step before); the second one, between about 180 and 370°C is associated to some thermal degradation reactions; the third one, between 370 and 520°C, is associated to the oxidation of the char [14], [15], [16], [17], [18]. The thermal degradation of the structural components of a lingo-cellulosic material provides for the breaking of the structure due to the high temperature, with a further liberation of some gaseous chemical species which burn when in contact with oxygen, giving this degradation phenomenon an overall exothermic character. The peak associated to the hemicellulose and cellulose degradation reactions are rather narrow and centered respectively around 250 and 290°C, while the lignin one is wider, centered around 350-400°C and covering the range 200-450°C. Following the thermal degradation, the char oxidation step. All the reactions occurring before lead to a structure porous enough to allows a high oxygen diffusion rate, allowing in turn oxidation and combustion reactions of the residue matter [14], [15], [16], [17], [18]. This step is obviously exothermic and the higher the surface area is, the faster this step is. The samples show a similar behavior looking at the first large peak, while a slightly different behavior in the char combustion step, where sample D (the finest one) stands out with its sharp peak. Furthermore, the peak temperature seems to follow a decreasing trend as the particle size increases. The pellet curve shows a more irregular comportment than the other ones.

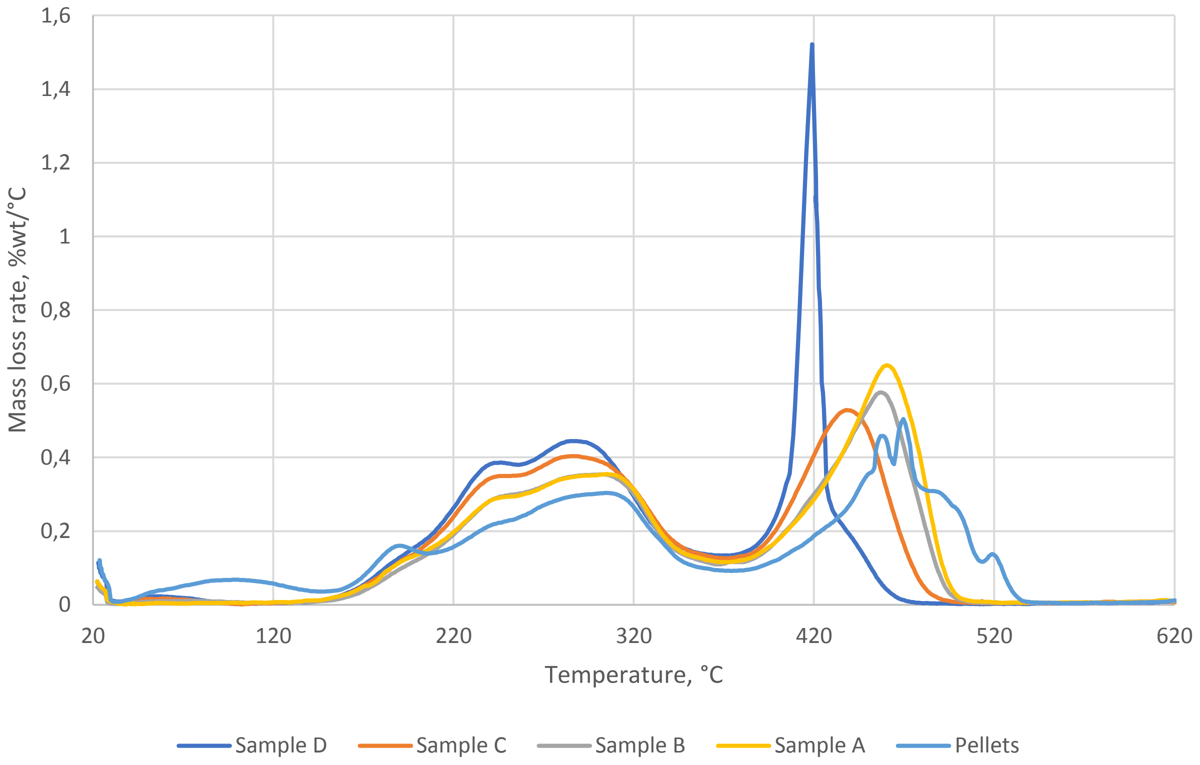

Figure 3.2 - Thermo-gravimetric analysis results.

3.1.3 Proximate analysis

The results from the TG analysis were used to calculate volatile matter, fixed carbon and ash content of the samples. They are shown in Table 3.2, together with the moisture content and the calorific value. The samples presented different volatile matter to fixed carbon ratio (VM/FC), therefore different reactivity, when heated up: sample B showed the highest reactivity, samples C and D similar reactivity, while sample A showed the lowest reactivity. The results of the proximate analysis were in line with those of Miranda et al [20] (also shown in Table 3.2), who analyzed the thermal behavior of four different olive residues. It seems the olive pomace sample analyzed in this work is closer to be formed mainly by olive pulp than olive pit, even though certain values are slightly different (VM and FC are higher in the Miranda's work, while the ash content is higher in this work).

Table 3.2 – Proximate analysis results. VM, FC and HHV were calculated on a dry-ash-free basis, ash content was calculated on a dry-basis.
[a] Calculated from the TG analysis.
[b] From [20].

Sample	Moisture (before drying) %wt	Moisture (after drying) %wt	Volatile matter %wt	Fixed carbon %wt	VM/FC	Ash %wt	HHV MJ/kg
Pellets	6.1[a]	-	72.8	11.7	6.2	15.5	23.7
A	5.4	0.6	66.0	25.5	2.3	8.5	22.9
B	5.0	1.0	79.3	6.7	11.8	14.0	24.4
C	6.4	1.0	76.0	13.3	5.7	10.7	23.7
D	6.0	1.1	74.5	17.1	4.4	8.3	22.6
Olive pit [b]	9-10	-	80.9	18.5	4.3	0.6	20.7
Olive pulp [b]	6-6.5	-	79.1	15.3	5.2	5.6	24.4
Residual olive cake [b]	5.5-6	-	77.8	17.9	4.3	4.3	23.3

3.1.4 Morphology

The SEM investigation was useful to understand how the particles are shaped and whether it was possible to identify some characteristic structures, such as olive pit, skin, pulp or kernel. The images obtained are shown in Fig. 3.3 (red arrows indicate some of the structures identified). Samples A and B showed a variety of particle shapes, more than the other two, but also particles with smoother surface, while the two finest samples seemed to have more jagged surfaces. In the SEM images, furthermore, it was possible to identify peculiar structures, reported in Table 3.3. The overall appearance seemed to suggest in the two coarsest samples the typical structures of the olive were preserved, being able to identify some parts of it (epicarp, mesocarp and endocarp); on the other hand, it was not possible to say the same for the two finest samples, in which the grinding led to the destruction of these structures, not recognizable anymore.

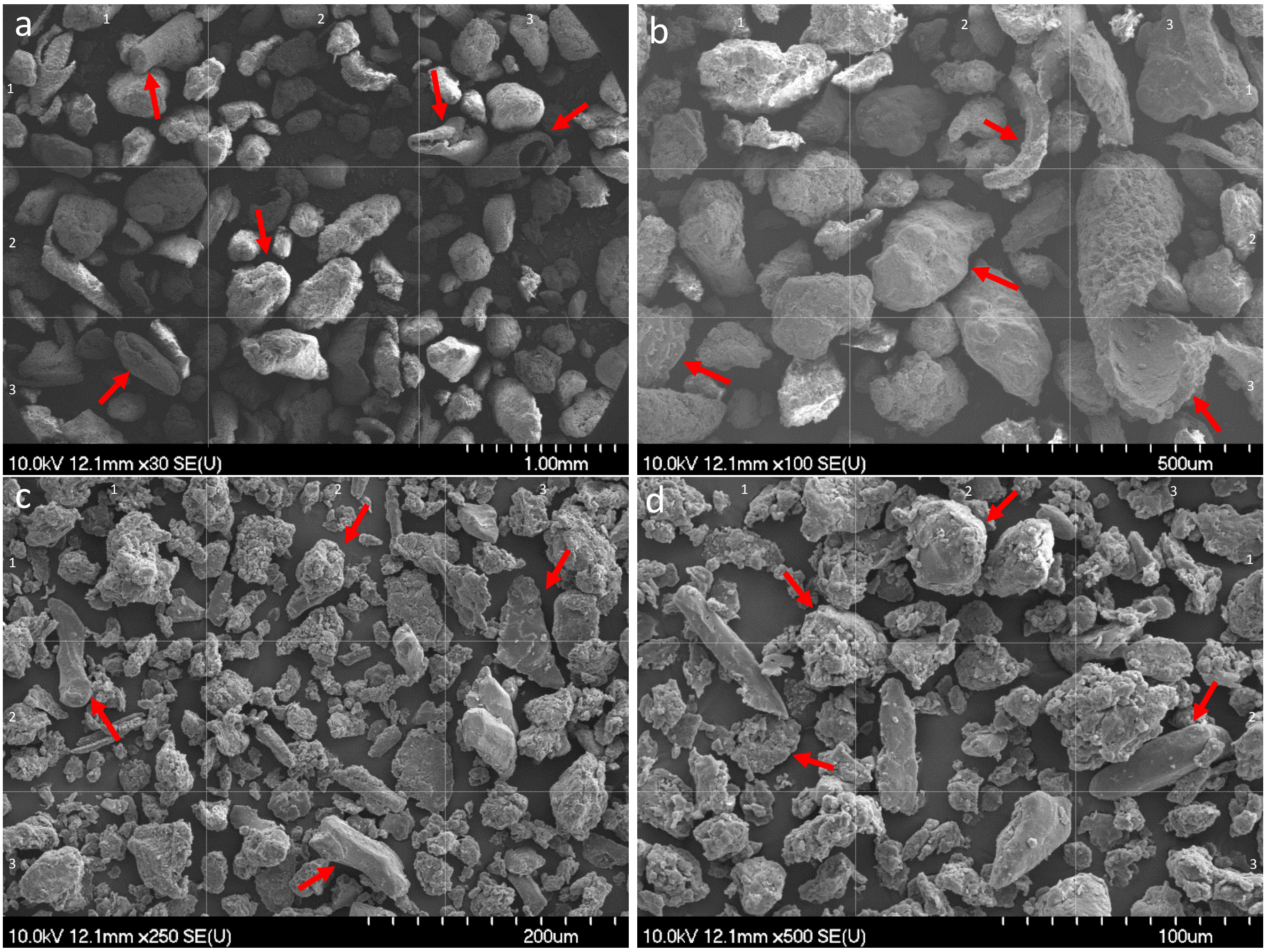

Figure 3.3 - SEM images of the four samples: sample A (a), sample B (b), sample C (c) and sample D (d). The images were chosen in order to be as much representative of the sample as possible.

3.1.5 Chemical characterization

Thanks to the solid-state NMR was possible to highlight any eventual differences in the chemical character among the samples. The ^{1}H and ^{13}C spectra are shown respectively in Fig. 3.4 and Fig. 3.5. It can be noticed how the signals are in general quite the same for all samples, with some relatively important changes in the pelletized sample. The graphs report the chemical shift expressed in ppm, which represent the ratio between the compound's chemical shift and the frequency used by the NMR apparatus (multiplied by 1 million), in order to disjoint the first from depending on the second one. In fact, the stronger the magnetic field, the higher a compound's chemical shift. So, instead of using Hz, ppm is used. The spectra from ^{1}H NMR did not show important peaks and the abscissa axe shows really low values (around the zero). The wideness is due mainly to the presence of dipole-dipole bonds and is typical of the ^{1}H spectra. ^{13}C NMR spectra show higher values on the abscissa axis, but still they did not show important differences between one and another. Knowing the integration range, it was possible to calculate the area under considered peaks. Results are shown in Fig. 3.6.

Table 3.3 - Supposed structures identified via the SEM investigation. Sectors numbers refer to column-row.

Structure in SEM images	Figure and sectors	Supposed structure in the olive
Broken pill	a: 1-1, 3-1, 2-2 b: 2-1, 3-3	The outer layer has a slightly honeycomb-like morphology, while the inner layer is smoother. The morphology is well preserved even if the sample has undergone a drying step (which potentially can modify it [21]). This layer may belong to the olive endocarp [22], since the honeycomb-like morphology can be attributed to the cells in the olive pulp (which are in direct contact with the outer layer of the endocarp), responsible for the storage of oily matter. Less numerous in sample B.
Wrap	a: 3-1, 1-2, 3-1	The outer layer is significantly irregular, while the inner layer is not visible because of the wrapping. These particles may come from the olive epicarp [22], the thin layer surrounding the olive which protect it from the outside dangers. The olive skin is made of a quite ductile material, so the irregularity of the outer surface could be due to some sort of deformation of the honeycomb-like surface.
Blunt particles	a: every sector b: every sector c: every sector d: every sector	Both small and big particles could belong to this type of structure. They show a quite blunt but irregular surface, may related to the olive pulp [23], since the mesocarp is the softer part of the olive and their appearance suggests a rather soft consistency.
Cylinder	a: 1-1	Way more different from any of the previous structures. The fibrous characteristics is evident, but the cylindrical-shape is peculiar. This structure may belong to an olive tree inflorescence that ended up in the olive pomace during the pressing step, since in the olive this kind of structure cannot be found [24].
Flat particles	b: 1-3 c: 1-1, 2-1, 2-2, 2-3, 3-1, 3-2 d: 1-1, 1-2, 2-2	The main characteristic of these structures is their flatness and their rather smooth surfaces. They do not seem to come from the further destruction of the “broken pills” because the smooth surface is significantly different. They may come from the inner layer of olive endocarp, that shows a really similar surface morphology [25].
Smooth particles	c: 2-3, 3-2 d: 2-1, 3-1	Not present in the previous samples, they may come from the destruction of the endocarp layer (more resistant to the grinding than the other olive constituents). Their very different shapes are maybe due to the fact they are made of a non-ductile material.
Agglomerates	c: every sector d: every sector	Formed by the smallest particles coming together to form an agglomerate, perhaps sticking onto bigger particles. They seem to have a very large surface area.

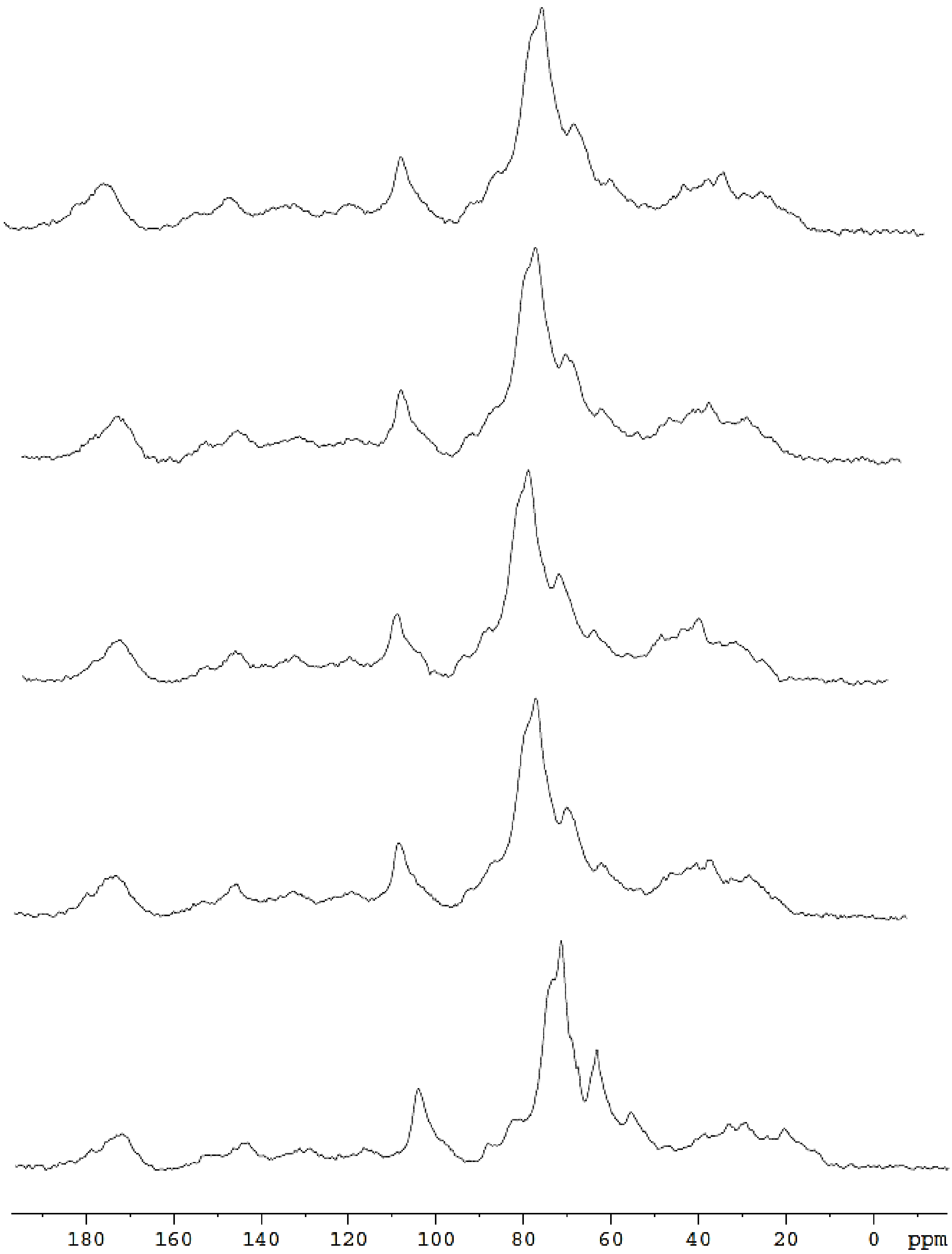

Figure 3.4 - ^{13}C NMR spectra. From the top: sample D, C, B, A and pellets. On the ordinate, the intensity of the signal from the detector.

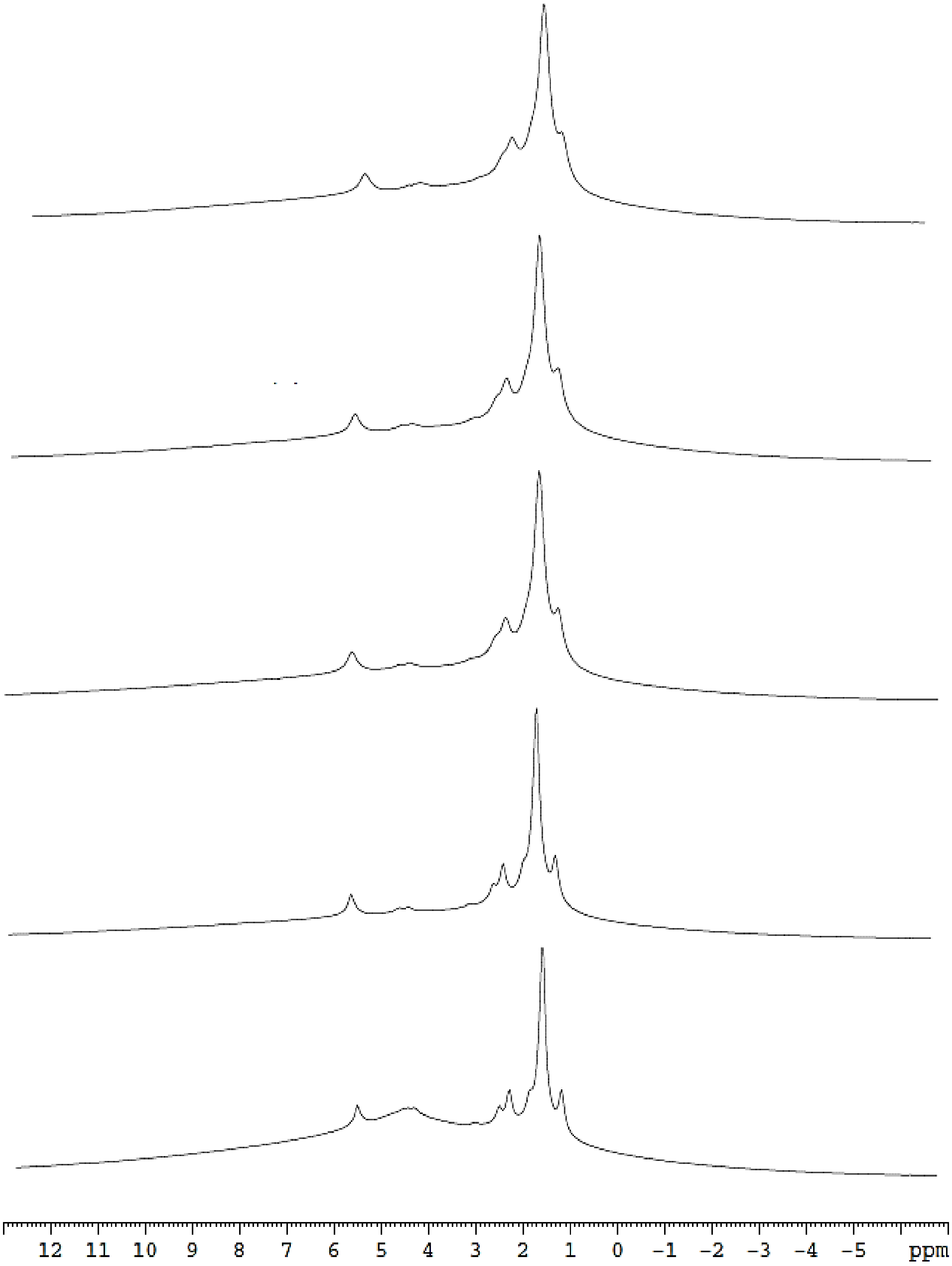

Figure 3.5 - ^{1}H NMR spectra. From the top: sample D, C, B, A and pellets. On the ordinate, the intensity of the signal from the detector.

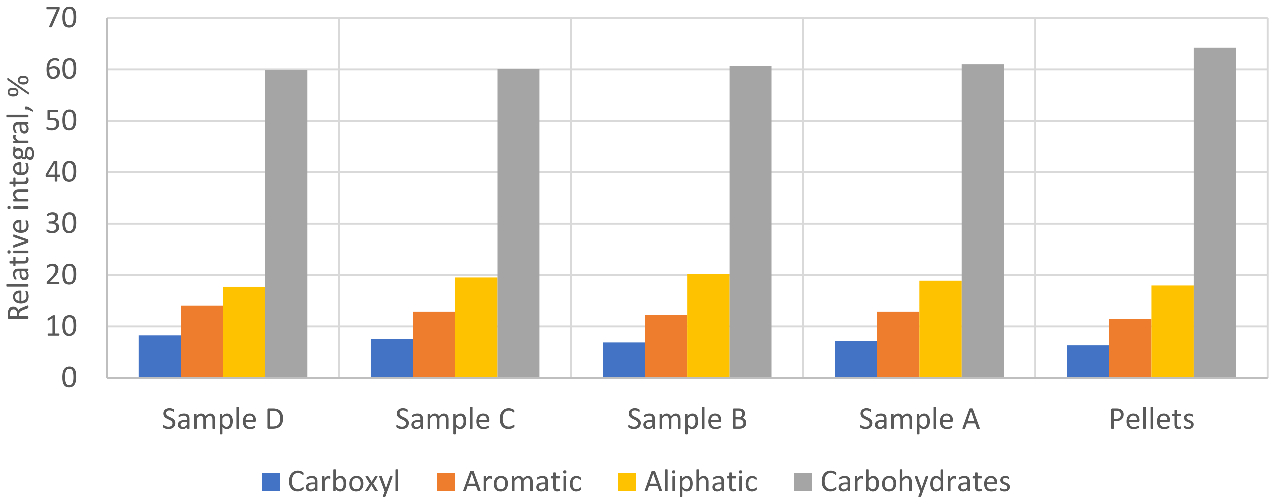

Figure 3.6 - Relative integrals from ^{13}C-NMR analysis. 4 characters were taken into analysis: presence of carboxyl group, aromatic ring, aliphatic chain or carbohydrates.

3.1.6 Bulk density

The results relative to the bulk density are shown in Table 3.4. Values' orders of magnitude were all the same; however, it seemed the samples C and D showed, in the case with vibrations, a bulk density lower than that of A and B samples'. Pellet bulk density was not influenced much by the presence of vibrations.

Table 3.4 - Bulk density results.

Sample	**Bulk density (no vibrations), kg/m^3**	**Bulk density (vibrations), kg/m^3**
Pellets	794	801
A	614	622
B	615	669
C	517	615
D	521	598

3.2 Explosibility and flammability analyzes results

3.2.1 Minimum Ignition Energy

The MIE analysis results are shown in Table 3.5. The MIE analysis showed the olive pomace samples were not sensitive to be ignited by an electrical spark with an associated energy lower than 1 J.

3.2.2 Minimum Auto Ignition Temperature

The MAIT analysis results are shown in Table 3.5. Values show the two finest samples were more thermally stable than the coarsest two, thus needing a higher temperature to reach the auto ignition. However, the mechanism of ignition was the same for all of them: there was no flame that instantaneously came out from the apparatus, but instead the coming-out flame appeared after 2-3 seconds from the injection of the powder, maybe due to the off-gases ignition into the chamber.

3.2.3 Explosion parameters

Results are shown in Table 3.5. The highest P_{max} value was relative to the sample B, while samples C and D showed quite similar values (even though speaking of P_{max}, a 0.3 bar difference is not negligible at all). Sample A's value was the lowest one. Concerning the $(dP/dt)_{max}$, the two finest samples were the ones with the highest values (in this case, a 3 bar/s difference is negligible), with sample B having an intermediate value and the coarsest one having the lowest value. Since the vessel used during the test was the same for all the four sample, K_{St} values followed the same trend as the $(dP/dt)_{max}$.

3.2.4 Minimum Explosible Concentration

Results are shown in Table 3.5. Values followed a decreasing trend as the particle size decreased, going from the highest value for the coarsest sample to the lowest value for the finest sample. In some tests, a double-bumped pressure-time profile was obtained. This is typical of the proximity of the MEC, where the first bump is due to the contribute of the igniters, while the second one to the contribute of the dust cloud ignition.

Table 3.5 - Results from the MIE, MAIT, MEC and explosion parameters study. The MIE apparatus highest spark energy which could be studied was 1000 mJ, thus a negative test obtained at 1000 mJ means the MIE is higher that that value.

Sample	**A**	**B**	**C**	**D**
MIE, mJ	> 1000	> 1000	> 1000	> 1000
MAIT, °C	500	480	540	550
P_{max}, bar	7.3	8.4	7.8	7.6
$(dP/dt)_{max}$, bar/s	84	166	258	255
K_{St}, bar m/s	23	45	70	69
MEC, g/m³	140	110	100	90

4. Discussion

4.1 Influence of the grinding-sieving step on samples behavior

All the results showed the four samples behaved differently from each other, even though they only went through a grinding-sieving step. Since the olive pomace is the solid residue coming from the olive oil extraction process, it is constituted by particles of all the olive tissues: exocarp (skin), mesocarp (pulp), endocarp (pit) and kernel. All these parts have different mechanical resistances and thus they might show different behavior to a grinding treatment. As a result, particles coming from the softer parts of the olive (pulp) will be more easily ground than the harder part (pit and kernel, mainly). Then, with a further sieving step, these two types of particles are separated from each other, leading to 2 fractions with different mechanical, physical and chemical behavior. In fact, Lammi et al [23] performed a dry fractionation by following flowchart-procedure, to obtain a stone-rich and a pulp-rich fractions from olive pomace only using various types of mill (knife, impact and ball mills) and a sieving system. Furthermore, Lammi et al [26] modified the flowchart-procedure used in their previous work and introduced an electrostatic separation to obtain smaller particles of a stone- and pulp-rich fractions, but still using only mechanical ways to separate the two fractions. Then, it is possible to assume that the grinding and sieving step of olive pomace led to four powders with potential different physical and chemical behaviors. This hypothesis was confirmed by all the analyzes.

4.1 Role of the sample composition

If the hypothesis according to which the samples different behavior of samples is due to the grinding-sieving step seemed confirmed, it is difficult to relate that to a changing chemical composition from sample to sample. As it can be seen in Fig. 3.5, the solid-state NMR did not enlighten any important differences in terms of aromatics, carbohydrates, carboxyl-group or aliphatic compounds. These compound classes were chosen in order to estimate a higher or lower presence of lignin, cellulose and hemicellulose, the main (structural) molecules in all lignocellulosic material, as olive pomace is. In Fig. 4.1 are shown the common structures of lignin, cellulose and hemicellulose. It is clear the NMR signal associated to aromatic molecules is mainly due to the presence of the lignin, while signals related to carbohydrates and aliphatic are mainly due to hemicellulose and cellulose. Carboxyl-group compounds are more present in hemicellulose, as well as lignin. This led to the conclusion that although the samples clearly showed different chemical and physical behaviors, this is not due to a change of composition.

The main cause of that different behavior between the four samples may have been a change in the specific areas associated to different particles. It is well known that as the particle size decreases, the surface specific area of particles increases, so the reactivity of a sample increases as its particle size shifts towards smaller diameter. However, if the sample is made of different mechanical-resiliency particles (as in the case of olive pomace) and the grinding-sieving step has been proved to be influencing on the different particle-sized samples, particle surface areas are associated to different tissues of the olive. For example, if a_T is the total surface area of sample *i*, the following equation is true:

$$a_{Ti} = a_{skin,i} + a_{pulp,i} + a_{pit,i} + a_{kernel,i}$$

where $a_{skin,i}$, $a_{pulp,i}$, $a_{pit,i}$ and $a_{kernel,i}$ are respectively the surface areas associated to the skin, pulp, pit and kernel particles in sample *i*. Even though the overall composition did not change so much, the chemical and physical behavior of each of these tissues is peculiar and different from the others. This reason could explain the different behavior of the samples.

Nevertheless, the lignocellulosic content of each of these parts cannot be related to the explosion behavior of the samples. As it can be seen in Fig. 4.2, in fact, a rapid and sudden heating of an olive pomace particle (ground pellet) leads to an overlapping of the typical and well-visible peaks associated to the thermal degradation reactions and combustion of char, which occur always in a biomass thermogravimetric analysis. It must be considered not even the maximum heating rate tested (100°C/min) was close to a particle heating rate during an explosion, so it is possible to assume during an explosion, this overlapping phenomenon is even more enhanced. Therefore, with the analyzes carried out in this work it is not possible to correlate the influence of the sample lignocellulosic content to its explosibility and flammability.

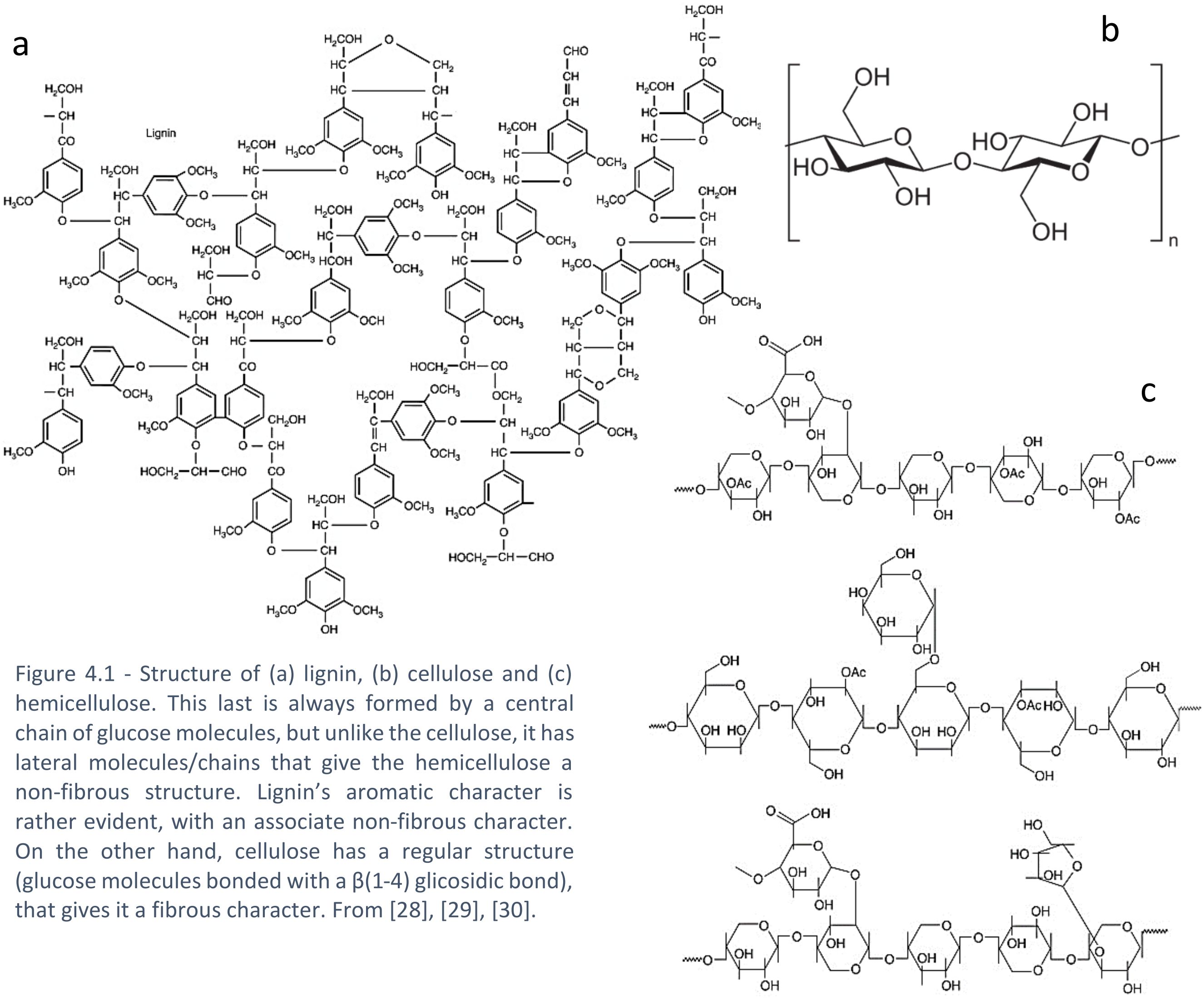

Figure 4.1 - Structure of (a) lignin, (b) cellulose and (c) hemicellulose. This last is always formed by a central chain of glucose molecules, but unlike the cellulose, it has lateral molecules/chains that give the hemicellulose a non-fibrous structure. Lignin’s aromatic character is rather evident, with an associate non-fibrous character. On the other hand, cellulose has a regular structure (glucose molecules bonded with a β(1-4) glicosidic bond), that gives it a fibrous character. From [28], [29], [30].

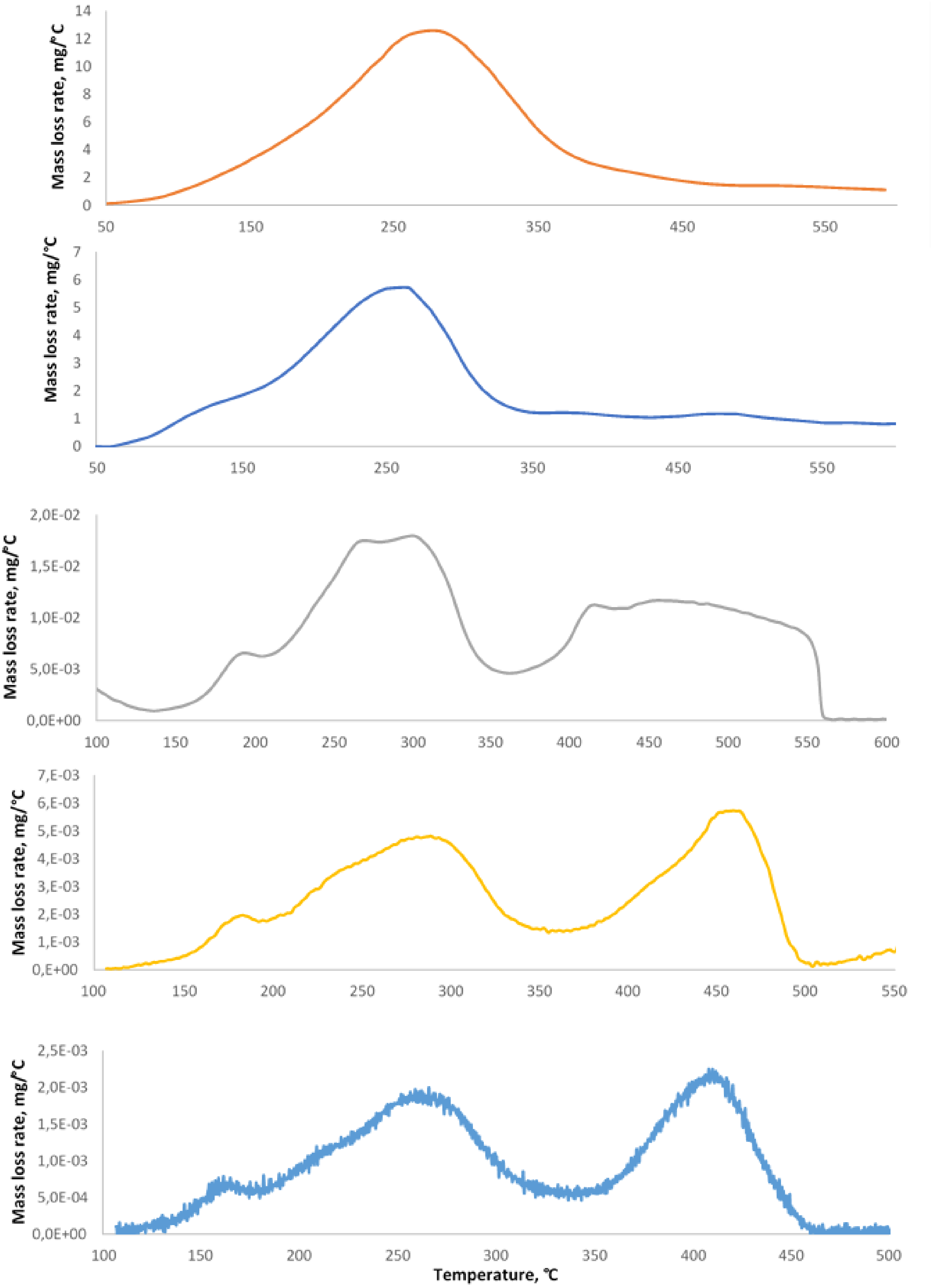

Figure 4.2 - TGA results carried out on a ground-pellet sample with different heating rates. From the top down: 100, 50, 10, 5 and 1 °C/min. The overlapping is clear by heating up the sample at 100 and 50°C/min, while from 10°C/min down the typical peaks are visible and no-more overlapped.

4.2 Influence of the explosion tests apparatus on samples explosibility

It is common knowledge the apparatus where analyzes are carried out influences enormously the results [30], [31], [32]. There are several parameters influencing the dust explosibility and flammability, more in general the chemical and physical behavior, that must be considered and that are related to the apparatus used for the experimental study. As Chawla et al [30] suggested, explosion parameters measurements must be related to the consciousness the procedure may affect the results, especially because the system is heterogeneous. In this case, the mean distance is way bigger than that of a homogeneous system, in which molecules are separated by only molecular distance and attain a quiescent system (to carve out the influence of the turbulence on the flame propagation) is more difficult [30]. For this very reason, several aspects have to be taken into account: eventual particle size modifications induced by the dispersion, homogeneity of the dust and even dispersion throughout the test apparatus.

First and foremost, it has been proved that the dust particle size is affected by its own dispersion. In fact, Bagaria et al [33], [34] resumed in their work how particles interact between each other, with the vessel walls and with the rebound nozzle walls during the dispersion, causing breakage of the particles that leads to a reduction of the particle size. This reduction has to be taken into account, in order to get some reliable results from the explosion tests. In Bagaria's work a comparison between 20-L, 36-L and 1-m3 chamber was made. The analyzed dusts showed a behavior correlated to their brittleness index (BI, which represents the resilience of a material, thus its capability to resists to mechanical stress): the higher was the BI, the higher was the particle breakage post-dispersion. Moreover, this particle size reduction seemed to be more enhanced in the 20-L and 36-L vessels than in the 1-m3 chamber. The reduction of the D50 in the 20-L vessel went also beyond 78% for one of the chosen materials (ascorbic acid, which showed also a really wider particle-size distribution after the dispersion in all the three vessels), while for lycopodium was 2.6%.

Secondly, a homogeneous distribution of the dust must be attained inside the chamber, but it seems to be sensitive to the type of used nozzle and to the concentration of the powder. Di Sarli et al [35] demonstrated the rebound nozzle (used in this work) allows to almost completely feed the dust into the chamber, but on the other hand leads to high turbulence level non-uniform in space, and to a non-uniform dust concentration. The perforated annular nozzle, instead, leads to a non-complete feeding of the dust into the chamber, but allows to reach low level of turbulence and a uniform dust concentration distribution.

Moreover, Di Sarli et al [36] showed in another work the concentration of dust injected into the chamber (equipped with a rebound nozzle) has important consequences on the dust concentration distribution: at low dust concentration (100 g/m3) high-concentration regions appear around the main vortex created during the dust dispersion; at high dust concentration (500 g/m3) dust sedimentation becomes important and very high-concentration regions appear around the nozzle; in the intermediate concentration region the concentration field seems to be more homogeneous. This aspect must be considered along with the not-so-high accuracy of the concentration value chosen for a specific trial, caused by the inevitable deposition of the dust (especially the finest one, which shows important cohesion forces) onto the walls of everything it comes in contact with: dust container, pipes, nozzle. This leads to a slightly decrease of the actual amount of powder dispersed within the chamber and thus a decrease of the representativity of the relative concentration value. That being said, using a range of dust concentrations (not close to each other) it is possible to estimate with a good accuracy degree the explosion parameters of the dust and to make comparisons between samples.

4.3 Influence of the ignition source on samples explosibility and flammability

A vitally important parameter that has to be taken into account and carefully chosen in explosibility and flammability analyzes is the ignition source. For all the four samples, in order to ignite the dust cloud, the ignition energy had to be furnished exclusively in the form of heat and not as electrical spark. In the 20-L chamber, in fact, the ignition source are countless sparks generated by the pyrotechnic igniters, so countless hot particles that came in contact with the dust particles to ignite the cloud, while in the BAM oven the dust cloud hit a hot surface. On the other hand, in the MIKE the dust cloud was not ignited by electrical spark of 1000 mJ. Furthermore, it emerged the igniters energy can affect greatly the explosibility of the samples, especially when it came to the explosibility analysis (MEC measurements). In fact, the MEC estimation demonstrated with different ignition energy, the response of the dust cloud was also different.

4.4 Explosibility of samples

The explosion parameters and the MEC results reported in Table 3.4 showed how explosibility of olive pomace dust is related to two main parameters, which are characteristic of the dust: the chemical composition (affecting the energetic content) and the particle size distribution (affecting the flame propagation rate). As expected, the $(dP/dt)_{max}$ (and also K_{St}) followed an increasing trend as the particle size decreased, while P_{max} showed a maximum for sample B, which had the maximum HHV and the maximum VM/FC ratio (respectively, higher energetic content and higher volatile matter over fixed matter). Moreover, in relation to the MEC values, it seemed the lower the particle diameter, the lower the minimum explosible concentration. As the particle size decreases, in fact, the surface area increases and in turn also the reaction rate does, as demonstrated by Semenova et al [37] with pine bark dust samples. Finest samples, thus, needed a lower concentration to ignite, while the lower surface area of the coarsest samples was responsible of the higher MEC values. Conclusively, $(dP/dt)_{max}$, K_{St} and MEC were mainly influenced by the particle size, while P_{max} was mainly influenced by energetic content and chemical reactivity (VM/FC). In Fig. 4.3 are reported the results of the explosion parameters tests: both $(dP/dt)_{max}$ and P_{max} are reported in function of the dust concentration. The wanted trend was obtained. In the first ascending part of each curve, the increasing concentration led to an increasing fuel/air ratio, where fuel is constituted by the gases released in the rapid heating of the particles during the explosion: the available amount of fuel is then bigger and bigger as the dust concentration increases and thus the adiabatic temperature (ideally) achievable is higher and higher, and in turn the achievable P_{max}. However, after a certain point (concentration correspondent to the P_{max}), the amount of off-gases is so high that their heat-sink character becomes more important than their energetic-release-contribute to the explosion, causing the decreasing trend as the dust concentration furtherly increases. For the same reason, $(dP/dt)_{max}$

graphs showed that type of trend: after a certain point, particles starts to absorb heat more than propagate the flame in the cloud, ending up with a decrease of the rate of pressure rise.

It would seem, also, the moisture content has had an important role in determining the explosion parameters of olive pomace dust. Silva Durán et al [38] worked on the same sample of olive pomace, obtaining comparable and interesting results from the explosion tests. Results are compared in Table 4.1. It is clear the higher moisture content in Silva Durán's work (who has not dried the samples) has led to a rather important decreasing of P_{max}, mainly influenced by the energetic content of the dust, whereas the (negligible) differences in K_{St} are mainly due to the different particle size distribution.

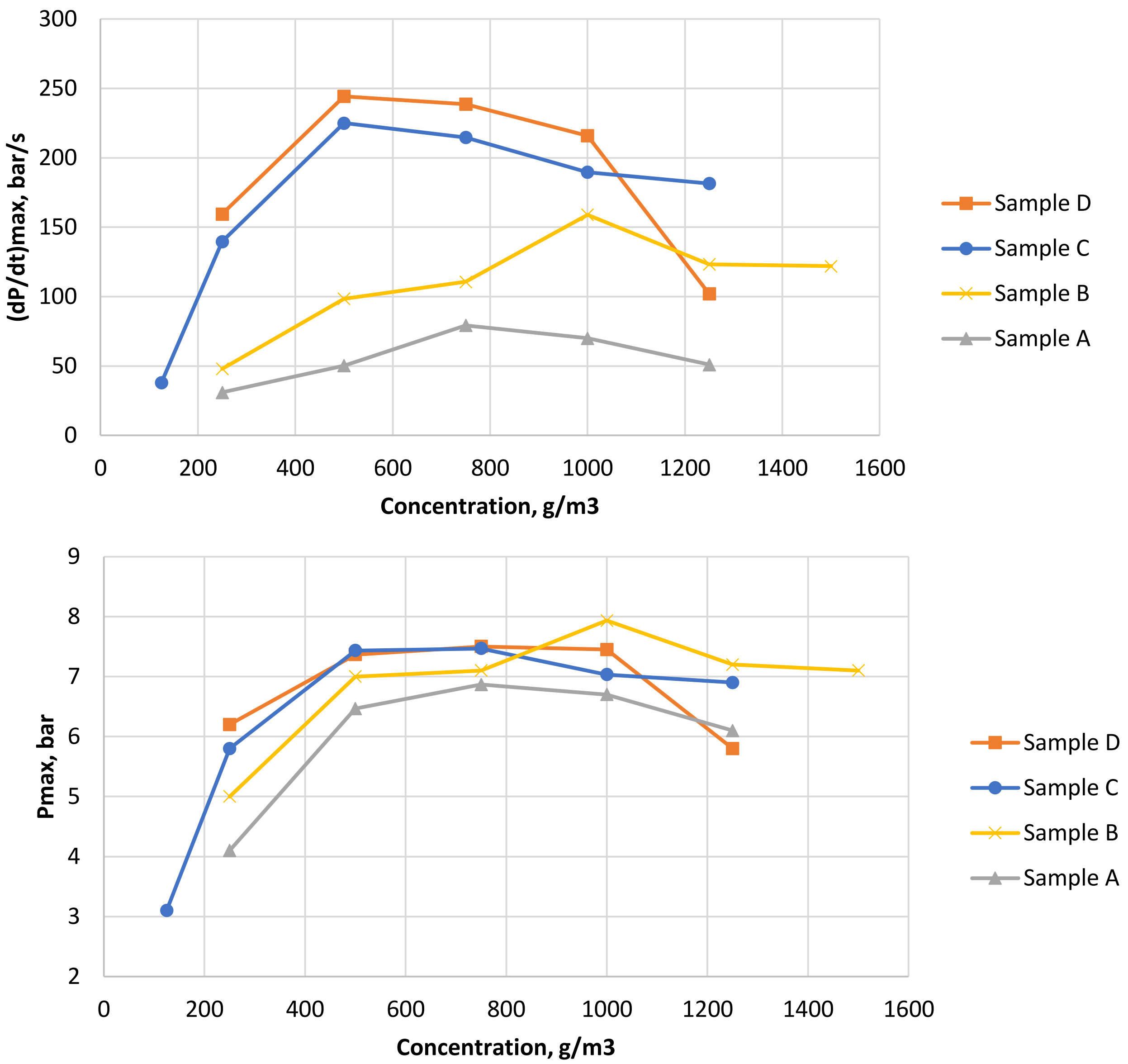

Figure 4.3 - Results from the explosion parameters tests. In the first graph it is reported the maximum rate of pressure rise reached during the tests in function of the dust concentration; in the second one the maximum pressure achieved during the explosion tests in function of the dust concentration

Table 4.1 - Comparison between Silva Durán's and this work's results concerning P_{max} and K_{St}.

Silva Durán's work				This work			
Fraction	**Moisture, %wt**	**P_{max}, bar**	**K_{St}, bar m/s**	**Fraction**	**Moisture, %wt**	**P_{max}, bar**	**K_{St}, bar m/s**
250-500 µm	6.89	5.9	21.4	**212-425 µm (sample A)**	0.6	7.3	23
<250 µm	6.39	6.8	49.4	**75-212 µm (sample B)**	1.0	8.4	45

4.5 Flammability of samples

The analysis to estimate the flammability of an olive pomace dust cloud was the MIT analysis, carried out with the BAM oven. In this apparatus, the dust cloud hit hot surface and eventually gets ignited, but also settles down at the bottom of the internal chamber. The settled dust has to ignite within 5 seconds to be considered as positive test. In Fig. 4.4 are reported the tested temperatures over the three studied dust volumes. It was noticed for temperatures from 510°C up, the two coarsest samples showed an instantaneous ignition classifiable as flash fire. Whenever the temperature was around 500°C or less, the flame coming out the metal flap was weaker and slower. Then, in the first case the dust cloud ignited as soon as it hit the hot surface, while in the second case the flame was caused by the ignition of the off-gases. As regards the two finest samples, the flame was never as instantaneous as in the case of the two others, but it was probably due to the ignition of the off-gases released by the settled dust and the excess of particulate matter. This analysis confirmed the hypothesis of low thermal reactivity of the two finest samples, as well as the high thermal reactivity of the other two. These results seemed to be in line with results from other works [39]. Furthermore, in Silva Durán's work [38], where a Godbert-Greenwald furnace (GG furnace) was used to evaluate olive pomace dust MIT, the trend seemed to be in line with the one obtained in this work with the BAM oven. In the GG furnace, the combustion chamber containing the hot surface is vertical: this allows to carve out the effect of the off-gases which can ignite in lieu of the dust. An ignition in the GG furnace is, then, only attributable to the ignition of the dust cloud and for this reason MIT values obtained in such apparatus are usually higher than the ones obtained in the BAM oven. Although the fractions analyzed were not the same (Silva Durán used four fractions: 1000-500, <500, <250 and <75 µm), the lowest MIT value was the one relative to the <250 µm fraction, not so different from the sample B of this work.

4.6 Minimum explosible concentration

In Fig. 4.5 are reported the results about the MEC analysis. The analysis carried out to determine the MEC showed significant relationship between probability of ignition and actual ignition. In a heterogeneous system as a dust cloud, the ignition can occur if the dust concentration is within the range of explosibility, if the ignition source provides enough energy and if particle size and composition of the material the dust is made out of made the dust combustible. However, even if these variables satisfy all the conditions, it is not enough speaking of dust explosion tests. Like it has been said in paragraph 4.2, the apparatus characteristics have a significant importance on results and it has been clearly noticed in the MEC analysis. Although the concentration was decreased, the P_m followed its own trend, as it can be seen, for example, in samples B and D, which showed some P_m values (relative to a concentration around 100 g/m^3) off the general trend. Furthermore, repeating the test more than two times means to increase the probability for the dust cloud to ignite. In fact, for example, fine particles might accumulate (completely randomly) in the zone around the igniters, giving an explosion whose P_m is higher than 1 barg, but also the apparatus influence might be less or more influencing in a test rather than in another one, leading to different Pm and different conclusions. This uncertainty might explain why MEC results between Silva Durán's work [38] (who used, by the way, the same 20-L vessel model used in this work but not the same physical apparatus) and this work were so different.

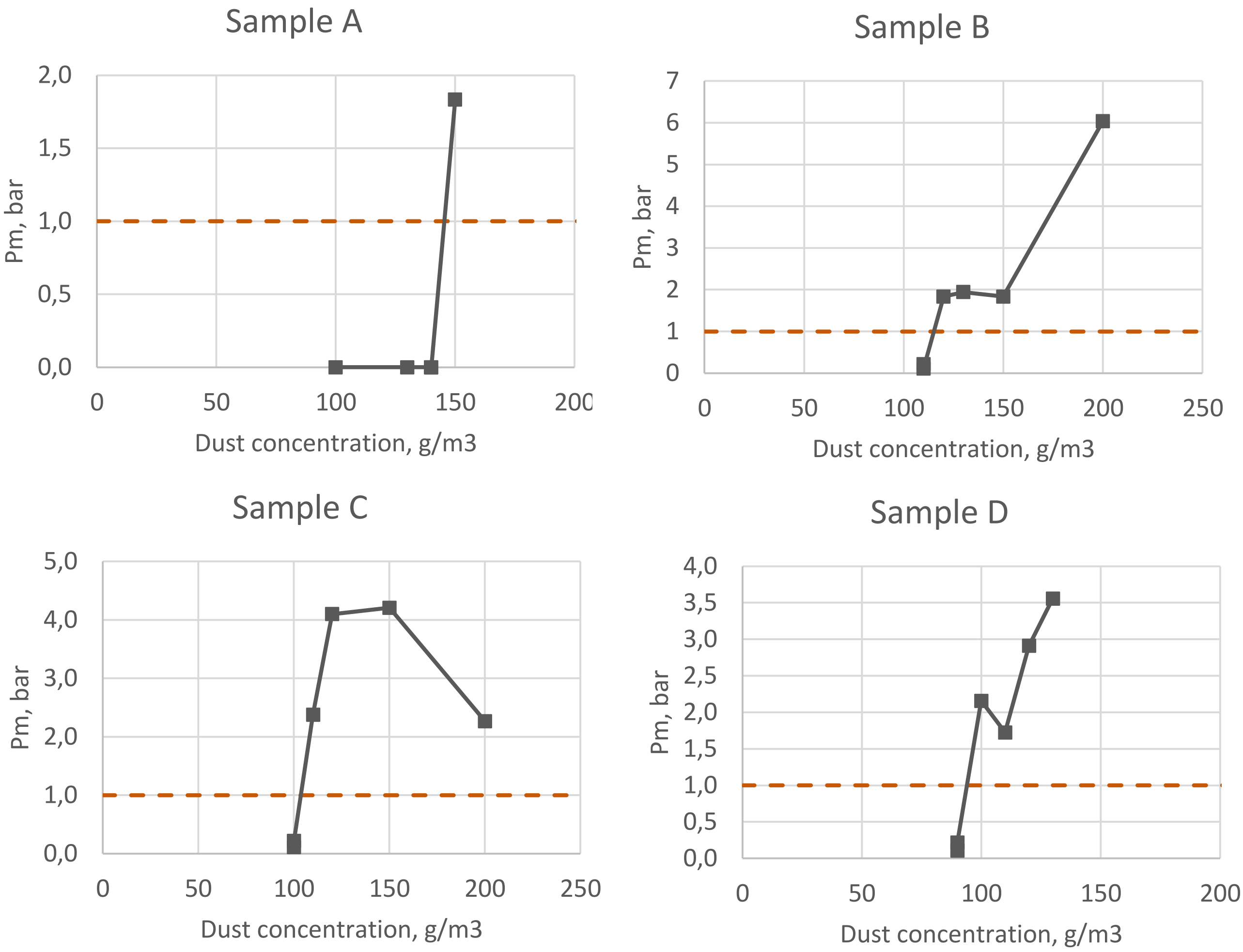

Figure 4.5 - MEC analysis results.

5. Conclusions

The hazard related to the handling of olive pomace and potential formation of olive pomace dust has been estimated studying its explosibility and its flammability when dispersed in air, forming dust clouds. Particle size did not have the major and absolute role in determining the explosion characteristics of the samples, but rather it seemed to be co-ruling over it with the heterogeneous nature of the sample itself.

Sample B showed in all analyzes a higher energetic content (HHV = 24.4 MJ/kg) and thermal reactivity (VM/FC = 11.8), which led it to cause the strongest explosion in terms of P_{max} (8.4 barg), while sample B and C showed lower energetic content (respectively, HHV = 23.7 and 22.6 MJ/kg) and thermal reactivity (VM/FC = 5.7 and 4.4, respectively), but higher K_{St} during the explosion test (respectively, 70 and 69 bar m/s). Sample A showed a low energetic content (HHV = 22.9 MJ/kg) as well as the lowest thermal reactivity (VM/FC = 2.3), even lower than the pellets' one. As regards the explosion tests, this sample showed the lowest P_{max} (7.3 barg) and the lowest K_{St} (23 bar m/s). It seems the grinding-sieving step had a deep influence on the behavior of the four dust samples.

The most influencing factor on the Minimum Explosible Concentration results was the particle size. Since the explosion severity (neither P_{max} nor $(dP/dt)_{max}$)) is not taken into account studying this parameter, only the particle size distribution influences the explosibility of the samples, in a rapid and quick combustion as an explosion. Values ranged between 90 (sample D) to 140 g/m^3 (sample A).

Olive pomace dust clouds showed to be rather sensitive to auto-ignite (causing fire classifiable as flash-fire) when exposed to high temperature, in particular to hot surfaces. Samples showed MAIT of 480 (sample B), 500 (sample A), 540 (sample C) and 550°C (sample D), comparable to results from other works. These results were in line with the VM/FC values, which allowed to estimate the thermal reactivity of the samples.

Samples did not show sensibility to be ignited by an electric spark with an associated energy of 1000 mJ, which allows to neglect the hazard related to olive pomace ignition by electrical sparks when designing of systems involving olive pomace.

Confronting results with Silva Durán's work (who studied the same olive pomace sample, but ground with a knife-mill and not dried) showed moisture content has an important role in determining the explosion parameters and flammability characteristics. A difference of about 5%wt in moisture content has potentially lead to a 20% reduction of the P_{max}, though leaving the K_{St} almost unaltered. Furthermore, a similar MIT trend was noticed between the two works.

This work would need to be filled with further information, in order to have an overall comprehension of which factors are really significant in olive pomace dust risk analysis and which ones are not. The first factor is the particle diameter, then the study of three/four more samples with different particle size (for instance, 100, 150, 250 and 500 µm) may be interesting and allow to elaborate a consistent trend for all the parameters studied in this work. Another important factor seemed to be the grinding-sieving step, then a complete study on grinding systems and how they influence morphology and behavior of samples will lead for sure to important conclusions. Furthermore, a dry fractionation of olive pomace to obtain a pulp- and pit-rich fractions might illuminate on the different behavior of the two main tissues of olives, and thus on the olive pomace dust behavior during explosion and fire.

6. References

[1] M. Barbanera, E. Lascaro, V. Stanzione, A. Esposito, R. Altieri and M. Bufacchi, 2016, Characterization of pellets from mixing olive pomace and olive tree pruning. *Renewable energy* 88, 185-191.

[2] https://it.wikipedia.org/wiki/Sansa_di_olive

[3] D. Eliche-Quesada and J. Leite-Costa, 2016, Use of bottom ash from olive pomace combustion in the production of eco-friendly fired clay bricks, *Waste Management* 48, 323-333

[4] Y. Yücel, 2011, Biodiesel production from pomace oil by using lipase immobilized onto olive pomace, *Bioresource Technology* 102, 3977-3980

[5] A. S. Stasinakis, I. Elia, A. V. Petalas and C. P. Halvadakis, 2008, Removal of total phenols from olive-mill wastewater using an agricultural by-product, olive pomace, *Journal of Hazardous Materials* 160, 408-413

[6] T. Akar, l. Tosun, Z. Kaynak, E. Ozkara, O. Yeni, E. N. Sahin and S. Tunali Akar, 2009, An attractive agro-industrial by-product in environmental cleanup: Dye biosorption potential of untreated olive pomace, *Journal of Hazardous Materials* 166, 1217-1225

[7] REN21, Renewable Energy Policy Network for the 21st Century, Renewables 2018: Global status report, available online at http://www.ren21.net/wpcontent/uploads/2018/06/178652_GSR2018_FullReport_web_final_.pdf

[8] V. Casson Moreno and V. Cozzani, (2015), Major accident hazard in bioenergy production, *Journal of Loss Prevention in the Process Industries* 35, 135-144

[9] A. Álvarez, C. Pizarro, R. García and J. L. Bueno, 2015, Spanish biofuels heating value estimation based on structural analysis, *Industrial Crops and Products* 77, 983–991

[10] Ogle. R. A., 2017, *Dust explosion dynamics*, Elsevier – Butterworth-Heinemann, Oxford, UK

[11] Amyotte P., 2013, *An introduction to dust explosions. Understanding the myths and realities of dust explosions for a safer workplace*, Elsevier – Butterworth-Heinemann, Oxford, UK

[12] M. A. Saeed, G. E. Andrews, H. N. Phylaktou and B. M. Gibbs, 2018, Burning Properties and Flame Propagation of varying size Pulverized Rice Husks. 12th International Symposium on Hazards, Prevention and Mitigation of Industrial Explosions (ISHPMIE), Kansas City, USA August 12-17 2018

[13] M. A. Saeed, G. E. Andrews, Herodotos N. Phylaktou and B. M. Gibbs, 2017, Flame speed and Kst reactivity data for pulverized corn cobs and peanut shells, *Journal of Loss Prevention in the Process Industries* 49, 880-887

[14] Wenhao Xie, Jianli Huang, Jingyong Liu, Yongjiu Zhao, Kenlin Chang, Jiahong Kuo, Yao He,

Jian Sun, Li Zheng, Wuming Xie, Shuiyu Sun, Musa Buyukada and Fatih Evrendilek, 2018, Assessing thermal behaviors and kinetics of (co-)combustion of textile dyeing sludge and sugarcane bagasse, *Applied Thermal Engineering* 131, 874–883

[15] Chamseddine Guizani, Khouloud Haddad, Mejdi Jeguirim, Baptiste Colin and Lionel Limousy, 2016, Combustion characteristics and kinetics of torrefied olive pomace, *Energy* 107, 453-463

[16] Colomba Di Blasi, 2008, Modeling chemical and physical processes of wood and biomass pyrolysis, *Progress in Energy and Combustion Science* 34, 47–90

[17] Candie Xie, Jingyong Liu, Wuming Xie, Jiahong Kuo, Xingwen Lu, Xiaochun Zhang, Yao He, Jian Sun, Kenlin Chang, Wenhao Xie, Chao Liu, Shuiyu Sun, Musa Buyukada and Fatih Evrendilek, 2018, Quantifying thermal decomposition regimes of textile dyeing sludge, pomelo peel, and their blends, *Renewable Energy* 122, 55-64

[18] Stefano Vecchio, Lorenzo Cerretani, Alessandra Bendini and Emma Chiavaro, 2009, Thermal Decomposition Study of Monovarietal Extra Virgin Olive Oil by Simultaneous Thermogravimetry/Differential Scanning Calorimetry: Relation with Chemical Composition, *Journal of Agricultural and Food Chemistry* 57, 4793–4800

[19] R. García, C. Pizarro, A. G. Lavín, J. L. Bueno, 2013, Biomass proximate analysis using thermogravimetry, *Bioresource Technology* 139, 1–4

[20] T. Miranda, A. Esteban, S. Rojas, I. Montero and A. Ruiz, 2008, Combustion Analysis of Different Olive Residues, *International Journal of Molecular Sciences*, 9, 512-525

[21] V. Marsilio, B. Lanza, C. Campestre and M. De Angelis (2000), Oven-dried table olives: textural properties as related to pectic composition, *Journal of the Science of Food and Agriculture* 80, 1271-1276

[22] B. Lanza and M. G. Di Serio (2015), SEM characterization of olive (Olea europaea L.) fruit epicuticular waxes and epicarp, *Scientia Horticulturae* 191, 49–56

[23] S. Lammi, N. Le Moigne, D. Djenane, N. Gontard and H. Angellier-Coussy (2018), Dry fractionation of olive pomace for the development of food packaging, *Bio-composites, Industrial Crops & Products* 120, 250-261

[24] F. Braadbaart, E. Marinova and A. Sarpaki (2016), Charred olive stones: experimental and archaeological evidence for recognizing olive processing residues used as fuel, *Veget Hist Archaeobot* 25, 415–430

[25] E. Marinova, J. M. A. van der Valk, S. Maria Valamoti and J. Bretschneider (2011), An experimental approach for tracing olive processing residues in the archaeobotanical record, with preliminary examples from Tell Tweini, Syria, *Veget Hist Archaeobot* 20, 471–478

[26] S. Lammi, A. Barakat, C. Mayer-Laigle, D. Djenane, N. Gontard, H. Angellier-Coussy, 2018, Dry fractionation of olive pomace as a sustainable process to produce fillers for biocomposites, *Powder Technology* 326, 44–53

[27] D. Watkins, Md. Nuruddin, M. Hosur, A. Tcherbi-Narteh, S. Jeelani, 2015, Extraction and characterization of lignin from different biomass resources, Journal of Materials Research and Technology 4, 26-32

[28] https://en.wikipedia.org/wiki/Cellulose

[29] https://www.sciencedirect.com/topics/chemistry/hemicellulose

[30] N. Chawla, P. R. Amyotte and Michael J. Pegg, 1996, A comparison of experimental methods to determine the minimum explosible concentration of dusts, *Fuel* 75, 654-658

[31] B. Janovsky, J. Skrinsky, J. Cupak and J. Veres, Coal dust, Lycopodium and Niacin used in hybrid mixtures with methane and hydrogen in 1 m^3 and 20 l chambers, 12th International Symposium on Hazards, Prevention and Mitigation of Industrial Explosions (ISHPMIE), Kansas City, USA August 12-17 2018

[32] A. Addo, A. G. Dastidar, J. R. Taveau, L. S. Morrison, F. I. Khan and P. R. Amyotte, Niacin, lycopodium and polyethylene powder explosibility in 20-L and 1-m3 test chambers, 12th International Symposium on Hazards, Prevention and Mitigation of Industrial Explosions (ISHPMIE), Kansas City, USA August 12-17 2018

[33] P. Bagaria, Q. Li, A. Dastidar and C. Mashuga, 2019, Classification of particle breakage due to dust dispersion, *Powder Technology* 342, 204–213

[34] P. Bagaria, J. Zhang, E. Yang, A. Dastidar, C. Mashuga, 2016, Effect of dust dispersion on particle integrity and explosion hazards, *Journal of Loss Prevention in the Process Industries* 44, 424-432

[35] V. Di Sarli, R. Sanchirico, P. Russo, A. Di Benedetto, 2015, CFD modeling and simulation of turbulent fluid flow and dust dispersion in the 20-L explosion vessel equipped with the perforated annular nozzle, *Journal of Loss Prevention in the Process Industries* 38, 204-213

[36] V. Di Sarli, P. Russo, R. Sanchirico, A. Di Benedetto, 2014, CFD simulations of dust dispersion in the 20 L vessel: Effect of nominal dust concentration, *Journal of Loss Prevention in the Process Industries* 27, 8-12

[37] O. Semenova, R. Pilão and C. Pinho, Influence of concentration and particle size on the explosibility of air pine bark dust mixtures, 11th Brazilian Congress of Thermal Sciences and Engineering, Curitiba, Brazil Dec 5-8

[38] Silva Durán M. A., 2019, Characterization of the deflagration parameters of the dust deriving from processing of the olive pomace, Master Thesis, Polytechnic of Turin, Turin, Italy

[39] R. C. Morrow, Prevention of fires and dust explosions within the biomass handling process, Pellet Fuel Institute (PFI) – Annual conference, Williamsburg, USA July 19-21 2015

7. Annex

7.1 Calibration of MIKE 3

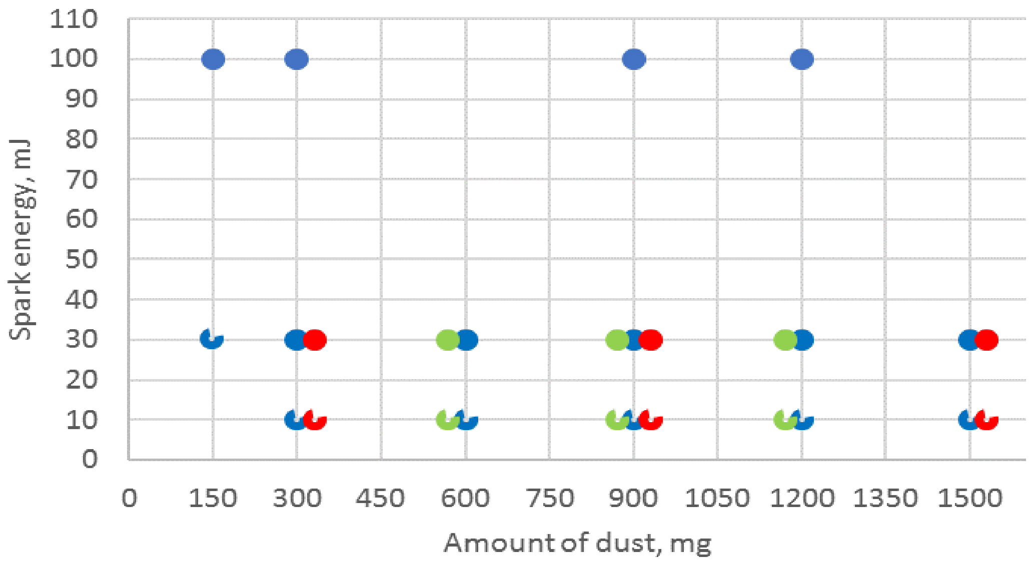

Figure 7.1- Results from calibration of MIKE 3 with Lycopodium. The complete circle stands for ignition; the non-complete circle stands for non-ignition.

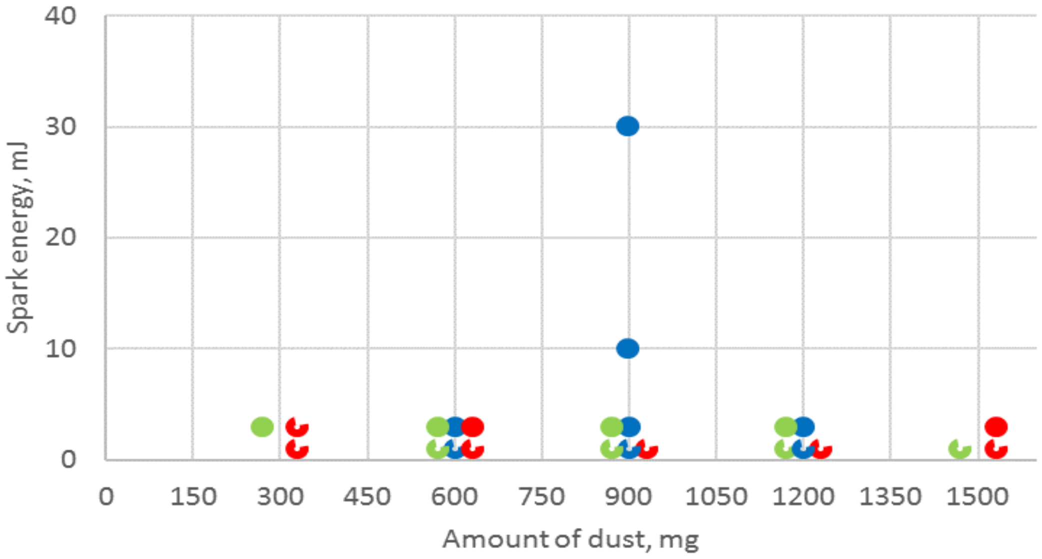

Figure 7.2- Results from calibration of MIKE 3 with CaRo13. The complete circle stands for ignition; the non-complete circle stands for non-ignition.

Table 7.1 – MIKE 3 calibration results checking with standard reference values.

	Range from standard, mJ	Range found, mJ
Lycopodium	10 to 30	10 to 30
CaRo13	3 to 10	3 to 10

7.2 Calibration of the 20-L vessel

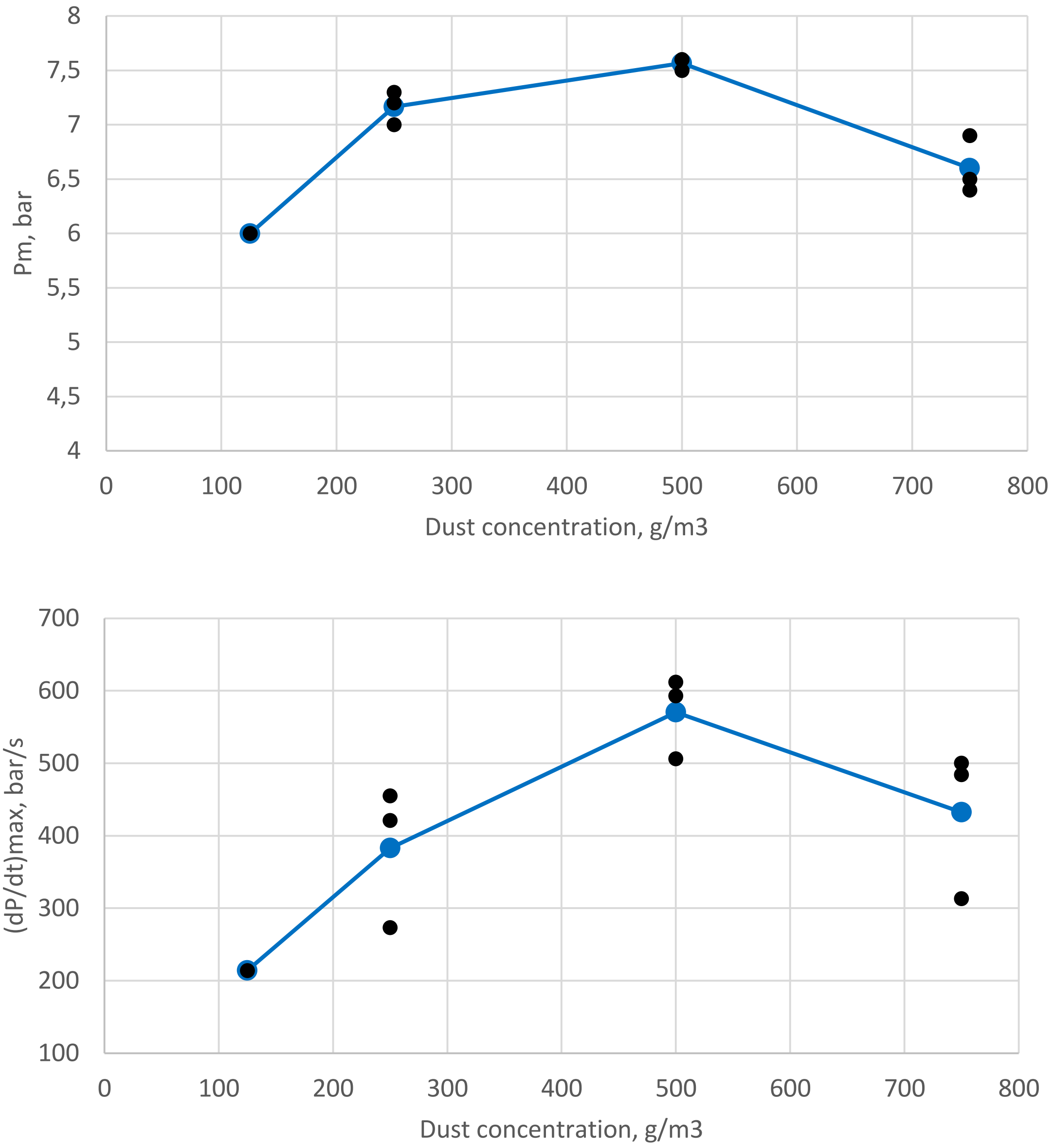

Figure 7.3- Results from calibration of the 20-L vessel, used for the explosion tests.

Table 7.2 – 20-L vessel calibration results checking with the standard reference values.

	From standard			**Found from calibration**		
	P_{max}, bar	**$(dP/dt)_{max}$, bar/s**	**K_{St}, bar m/s**	**P_{max}, bar**	**$(dP/dt)_{max}$, bar/s**	**K_{St}, bar m/s**
Lycopodium	7.0	555	151	7.6	570	155

Allowed error range		**Error range from calibration**	
P_{max}, %	**K_{St}, %**	**P_{max}, %**	**K_{St}, %**
±10	±20	+8.6	+2.6

7.3 Calibration of the BAM oven

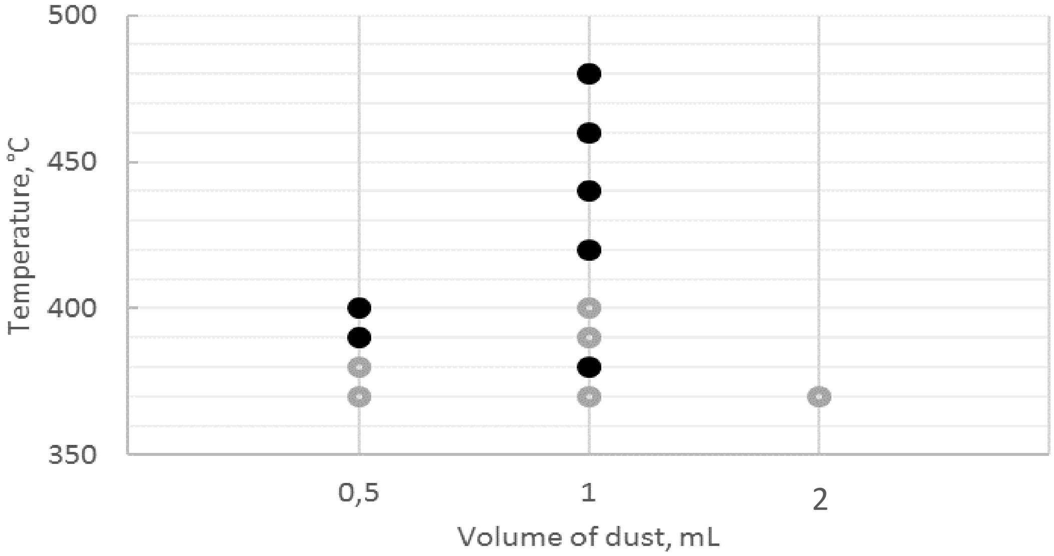

Figure 7.4 - Results from calibration of the BAM oven with Lycopodium.

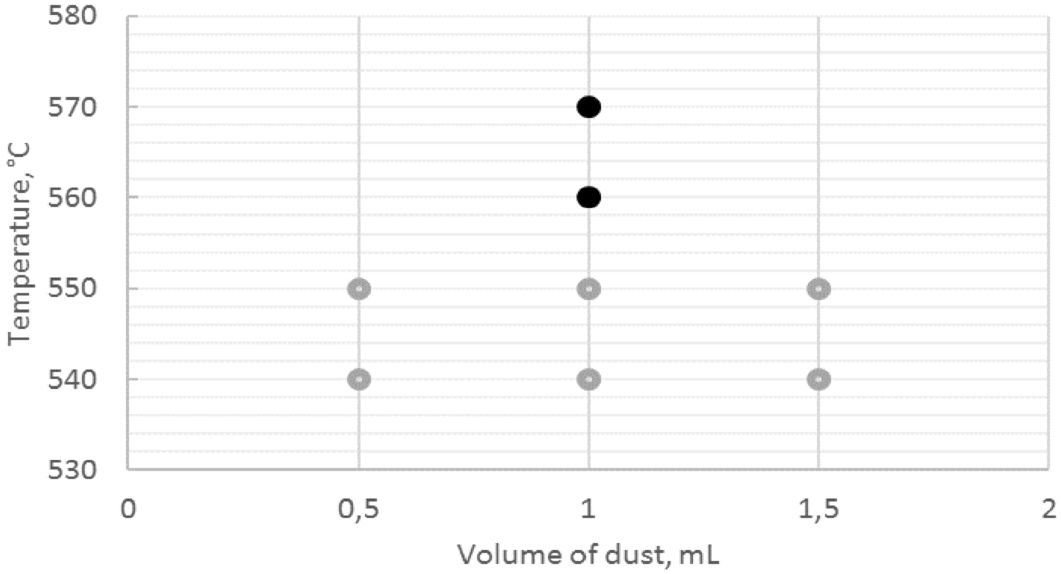

Figure 7.5 - Results from calibration of the BAM oven with Pittsburgh coal.

Table 7.3 – BAM oven calibration results checking with the standard reference values.

	MIT from standard, °C	**MIT found, °C**	**ΔT allowed, °C**	**ΔT found, °C**
Lycopodium	410	380	30	30
Pittsburgh coal	570	560	30	10

7.4 List of symbols and acronyms

MAIT	Minimum Auto Ignition Temperature	D_{50}	Diameter corresponding to the 50% (cumulative) of the particles
MIE	Minimum Ignition Energy	D_{90}	Diameter corresponding to the 90% (cumulative) of the particles
MEC	Minimum Explosible Concentration	a_{ti}	Total specific area associated to sample *i*
P_{max}	Maximum pressure achieved in an explosion test (2-3 series)	$a_{skin,i}$	Total specific area associated to the skin particles of sample *i*
$(dP/dt)_{max}$	Maximum pressure rise rate achieved in an explosion test (2-3 series)	$a_{pulp,i}$	Total specific area associated to the pulp particles of sample *i*
K_{St}	Explosion index	$a_{pit,i}$	Total specific area associated to the pit particles of sample *i*
TGA	Thermo-Gravimetric Analysis	$a_{kernel,i}$	Total specific area associated to the kernel particles of sample *i*
VM	Volatile Matter	P_{ex}	Explosion overpressure
FC	Fixed Carbon	P_m	Corrected explosion overpressure
M_i	Initial mass (TGA)	$(dP/dt)_m$	Rate of pressure rise (of a series)
M_d	Mass associated to the dehydration, air atmosphere (TGA)	P_d	Expansion overpressure
M_d'	Mass associated to the dehydration, inert atmosphere (TGA	t_d	Time-delay of the outlet valve
ASH	Ash content (TGA)	t_v	Ignition delay time
MC	Moisture Content (TGA)	t_1	Duration of combustion
D_{10}	Diameter corresponding to the 10% (cumulative) of the particles	t_2	Induction time

8. Acknowledgements

This work was developed during an exchange program between Polytechnic of Turin (Turin, Italy) and Dalhousie University (Halifax, Canada). I thank these two institutions for letting me be part of it, as well as Paul Amyotte for having me as visiting student in his research team and Albert Addo to have trained and helped me thoughout this work. I thank Gaëlle Ducom and Mathieu Gautier from the DEEP Laboratory (Laboratoire Déchets Eaux Environnement Pollutions) of INSA Lyon for providing me with the olive pomace sample used in this work. I thank Daniel Chevalier and his team from the Minerals Engineering Centre of Dalhousie University for their fundamental help with the preparation of the sample. I acknowledge Dr. Ulrike Werner-Zwanziger from the NMR-3 at the Chemistry Department at Dalhousie University and the Institute for Research in Materials for the acquisition and analysis of the NMR data.